Ref. Ares(2026)4856291 - 13/05/2026

GO-VIKING

Research and Innovation Action (RIA)

This project has received funding from the Euratom research and innovation programme 2021-2025 under Grant Agreement No 101059603

Start date : 2022-06-01 Duration : 48 Months

TITAN simulation results

Authors : Federico BARAGLIA (EDF), William Benguigui (EDF R&D, Fluid Mechanic division, 6 Quai Watier 78400 Chatou, France, IMSIA - UMR 9219 EDF/ENSTA/CNRS - 7 boulevard Gaspard Monge 91120 Palaiseau, France), Daniele Vivaldi (ASNR, Cadarache, St Paul-lez-Durance, BP3, 13115, France), Sina Tajfirooz (NRG PALLAS, Westerduinweg 3, 1755 LE Petten, The Netherlands), Kevin Zwijsen (NRG PALLAS, Westerduinweg 3, 1755 LE Petten, The Netherlands), Constantinos Katsamis (EDF Energy R&D UK, 11 Bressenden Place, London, SW1E 5BY, United Kingdom), Ehimen Iyamabo (EDF Energy R&D UK, 11 Bressenden Place, London, SW1E 5BY, United Kingdom), Théo Ondoua (EDF R&D, Fluid Mechanic division, 6 Quai Watier 78400 Chatou, France), Fanny Beltran (EDF R&D, Fluid Mechanic division, 6 Quai Watier 78400 Chatou, France), Samuel Gaucher (EDF R&D, Fluid Mechanic division, 6 Quai Watier 78400 Chatou, France)

GO-VIKING - Contract Number: 101059603

Project officer: Angelgiorgio IORIZZO

Document title	TITAN simulation results
Author(s)	Federico BARAGLIA, William Benguigui (EDF R&D, Fluid Mechanic division, 6 Quai Watier 78400 Chatou, France, IMSIA - UMR 9219 EDF/ENSTA/CNRS - 7 boulevard Gaspard Monge 91120 Palaiseau, France), Daniele Vivaldi (ASNR, Cadarache, St Paul-lez-Durance, BP3, 13115, France), Sina Tajfirooz (NRG PALLAS, Westerduinweg 3, 1755 LE Petten, The Netherlands), Kevin Zwijsen (NRG PALLAS, Westerduinweg 3, 1755 LE Petten, The Netherlands), Constantinos Katsamis (EDF Energy R&D UK, 11 Bressenden Place, London, SW1E 5BY, United Kingdom), Ehimen Iyamabo (EDF Energy R&D UK, 11 Bressenden Place, London, SW1E 5BY, United Kingdom), Théo Ondoua (EDF R&D, Fluid Mechanic division, 6 Quai Watier 78400 Chatou, France), Fanny Beltran (EDF R&D, Fluid Mechanic division, 6 Quai Watier 78400 Chatou, France), Samuel Gaucher (EDF R&D, Fluid Mechanic division, 6 Quai Watier 78400 Chatou, France)
Number of pages	37
Document type	Deliverable
Work Package	WP4
Document number	D4.6
Issued by	EDF
Date of completion	2026-05-12 17:38:56
Dissemination level	Public

Summary

Model preparation and simulation results for the TITAN experiment

Approval

Date	By
2026-05-12 17:41:02	William BENGUIGUI (EDF)
2026-05-13 14:25:33	Papukchiev ANGEL (GRS)

GO VIKING

D4.6 Titan Simulation Results

Numerical simulation of an air-water flow across a triangular tube bundle.

Version N°2
May/2026

William Benguigui[1,2], Daniele Vivaldi[3], Sina Tajfirooz[4], Kevin Zwijsen[4], Constantinos Katsamis[5], Ehimen Iyamabo[5], Théo Ondoua[1], Fanny Beltran[1], Samuel Gaucher[1]

[1]EDF R&D, Fluid Mechanic division, 6 Quai Watier 78400 Chatou, France
[2]IMSIA – UMR 9219 EDF/ENSTA/CNRS – 7 boulevard Gaspard Monge 91120 Palaiseau, France
[3]ASNR, Cadarache, St Paul-lez-Durance, BP3, 13115, France
[4]NRG PALLAS, Westerduinweg 3, 1755 LE Petten, The Netherlands
[5]EDF Energy R&D UK, 11 Bressenden Place, London, SW1E 5BY, United Kingdom

Funded by
the European Union

Disclaimer

The content of this report reflects only the author's view. The European Commission is not responsible for any use that may be made of the information it contains.

Document information

Grant Agreement / Proposal ID	101060826
Project Title	Gathering expertise On Vibration ImpaKt In Nuclear power Generation
Project Acronym	GO-VIKING
Scientific Coordinator	Angel Papukchiev, mailto:Angel.Papukchiev@grs.de, GRS, Kevin Zwijsen, mailto: zwijsen@nrgpallas.com
Project starting date (duration)	1st June 2022 – 31st May 2026 (48 Months)
Related Work Package	WP4
Related Task(s)	4.3
Lead Organisation	EDF
Contributing Partner(s)	EDF R&D/IMSIA. EDF-E, VTT, NRG PALLAS, ASNR
Due Date	M42 (30.11.2026)
Submission Date	15.03.2026
Dissemination level	PU

History

Date	Version	Submitted by	Reviewed by	Comments
15.03.2026	1.0	W.Benguigui	A. Papukchiev & K. Zwijsen	
12.05.2026	2.0	W.Benguigui	A. Papukchiev & K. Zwijsen	

Table of contents

1. Experiment 8
1.1 Mock-up 8
1.2 Rigid configuration 9
1.3 Flexible configurations 9
2. Numerical modeling 11
2.1 EDF R&D 11
2.2 NRG PALLAS 12
2.3 EDF UK 12
2.4 ASNR 14
2.5 Sum-up of the numerical approaches 15
3. Calculation domain & Mesh 16
3.1 EDF R&D 16
3.2 NRG PALLAS 17
3.3 ASNR 17
3.4 EDF UK 18
3.5 Sum-up of the calculation domains & Mesh 19
4. Rigid configuration 19
4.1 Qualitative analysis of the flow through numerical simulation 19
4.1.1 Qualitative analysis from EDF R&D 21
4.2 Void fraction: Numerical vs Experimental results 23
4.3 Fluid forces: Numerical vs Experimental results 23
5. Flexible configuration 26
5.1 EDF R&D contribution 26
5.2 ASNR contribution 27
5.3 NRG PALLAS Contribution 29
5.4 EDF UK Contribution 31
6. Conclusion 35

List of figures

Figure 1 Sketch of Titan Facility 8

Figure 2: Sketch of the two flexible configurations with 2 and 7 flexibles tubes. 10

Figure 3: Experimental results of two-phase flow-induced vibration in TITAN. RMS vibration is presented with two different units : %D corresponding to the ratio between displacement and tube diameter and in mm. 10

Figure 4: Calculation domain and view of the mesh from EDF R&D. 16

Figure 5: cross sections of the computational domain. (a) Full domain in the x-y plane. (b) Left: mesh in the vicinity of the tube bundle. 17

Figure 6 VIew of the mesh in the tube bundle used by ASNR. 18

Figure 7: Zoomed-in sections of the computational grid used for the TITAN cases. 18

Figure 8 Instantaneous void distribution along the tube bundle for Case 2 from each partner (from 0% (blue) to 100% (red)). 20

Figure 9 Averaged void distribution along the tube bundle for Case 2 from each partner (from 0% (blue) to 100% (red)). 20

Figure 10 Sensitivity analysis on preliminary computations to the reduced length with periodicity on Case 1 on force spectra (a), averaged void distribution with the full domain along tubes for Case 3 (b) and Case 4 (c) 21

Figure 11: Instantaneous (top) and averaged (bottom) void fraction distribution along the tube bundle from EDF R&D. 22

Figure 12 Void fraction profile along x at the optical probal altitude from each partner for each case. 23

Figure 13 Cross comparison of PSD force spectra for drag and lift direction for each case. 25

Figure 14 Displacement in %D of each cylinder from the simulation compared to the RMS displacement from the experiment for configuration n°11. 26

Figure 15 calculated displacement of tubes 4 and 7 (the tube numbering refers to configuration 11 28

Figure 16 PSD of the calculated displacement of tubes 4 and 7 (the tube numbering refers to configuration 11). 28

Figure 17: Power spectral density (PSD) of the drag force (left) and lift force (right) acting on the tube. Comparison between the results obtained with the original mesh (bottom) and the improved mesh (top) for Test 2. 30

Figure 18: History of the tube displacement (left) and corresponding power spectral density (PSD) of the displacement (right). The root-mean-square (RMS) tube displacement is 0.9% of the tube diameter, with a dominant vibration frequency of approximately 20 Hz. 30

Figure 19: Configuration 11 - Comparison of the RMS amplitude of vibration versus flow pitch velocity between the simulations and the experiment data. 32

Figure 20: Configuration 11 – Case 2: Plot of the timeseries of the displacement (normalised by the diameter) of Tubes 4 and 7. 32

Figure 21: Configuration 11 – Case 2: PSD of the displacement of Tubes 4 and 7 33

Figure 22: Configuration 11 – Case 4: PSD of the displacement of Tubes 4 and 7 33

Figure 23: Configuration 11 – Case 6: PSD of the displacement of Tubes 4 and 7. 34

Figure 24: Configuration 3 – Case 3: Plot of the timeseries of the displacement (normalised by the diameter) of Tubes 4 to 10. 34

Figure 25: Configuration 3 – Case 3: PSD of the displacement of Tubes 4 to 10. 35

List of tables

Table 1: Properties of rigid configuration tests 9

Table 2: Sum-up of the numerical approaches from each partner 15

Table 3 Sum up of the calculation domains & mesh from each partner 19

Table 4: Configuration 3 – Case 3: Comparison of RMS vibration amplitude between the experiment and the numerical simulation 34

Abbreviations and Acronyms

Acronym	description
CFD	Computational Fluid Dynamic
FIV	Flow-Induced Vibration
GO-VIKING	Gathering expertise On Vibration ImpaKt In Nuclear power Generation
HRIC	High Resolution Interface Capturing

LES	Large Eddy Simulation
URANS	Unsteady Reynolds Averaged Navier Stokes
VOF	Volume Of Fluid
WP	Work Package

Summary

The present work is dedicated to the simulation of the TITAN experiment, an air-water flow across a triangular tube bundle. Four partners present simulations with different codes, numerical setup or models on the rigid configuration for different two-phase flow pattern and for a flexible configuration to take into account the resulting vibration.

Keywords

Key words: Two-phase flow, tube bundle, CFD, numerical simulation, flow-induced vibration, rotated triangular arrangement

Introduction

The GO-VIKING project investigates FIV phenomena occurring in nuclear reactors under single and two-phase flow conditions. The focus of WP4 of the project is on FIV phenomena induced by two-phase flows, such as in steam generator. The present document, as part of WP4, reports simulations of experiments performed at CEA Saclay (France) on a triangular tube bundle facility, named TITAN, subjected to an air-water cross-flow. The triangular bundle consists of 30 tubes with two columns of half-tubes at both lateral plates to minimize wall effects with a pitch ratio of P/D = 1.44, representative of French steam generators. A rigid and a flexible configuration are simulated by four different partners with different numerical approaches in 4 different codes. Numerical approaches and calculation domains are presented, then rigid configuration results are discussed and finally, some calculations in flexible configuration are described.

1. Experiment

The experimental rig TITAN is located in the CEA/SEMT/DYN laboratory and is used to perform FIV tests on a rotated triangular tube bundle subjected to a two-phase air-water flow (Figure 1). TITAN is connected to the air-water loop of the RESEDA platform, which allows to reproduce flow conditions typically found in nuclear steam generators. The reader is referred to [1, 2] for a detailed description of the rig.

1.1 Mock-up

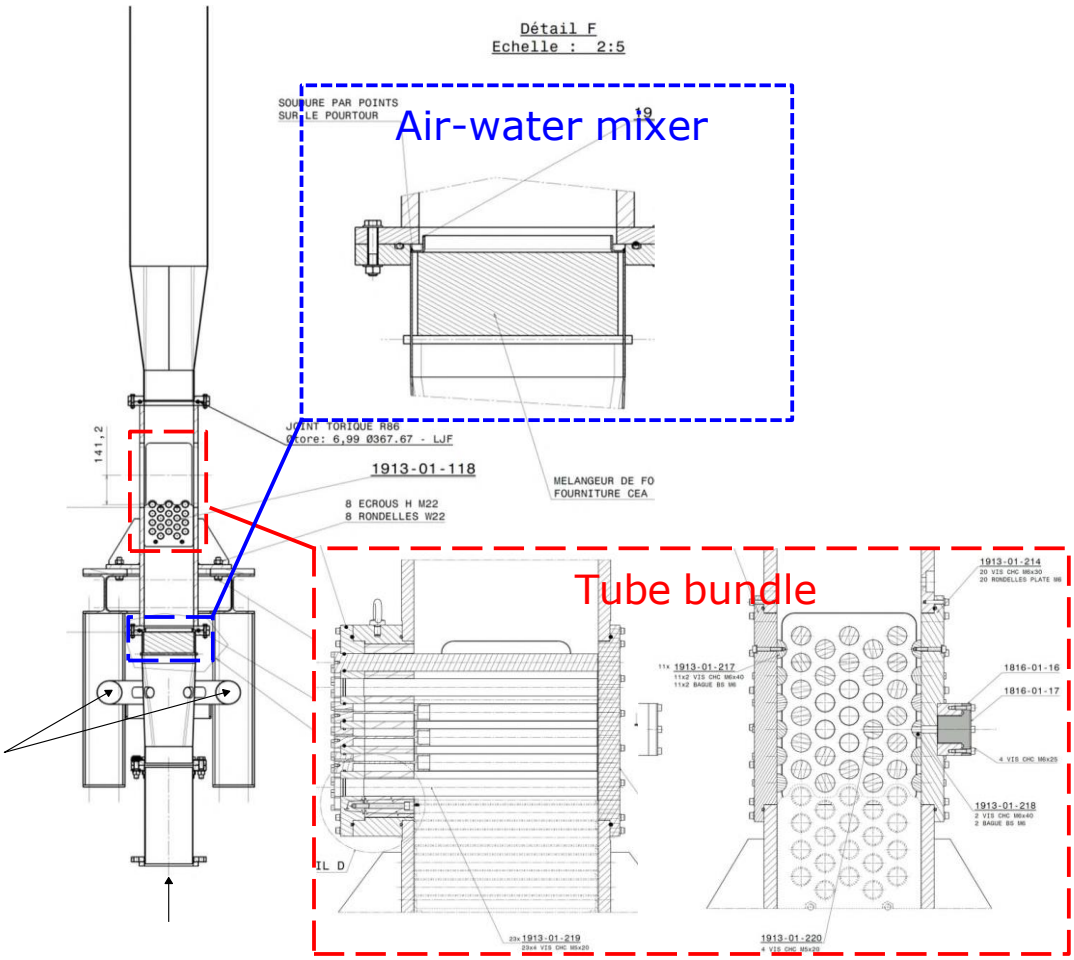

Figure 1 Sketch of Titan Facility

The two-phase flow loop includes a water centrifugal pump with maximum delivery capacity of 1100 m3/h and an air compressor which delivers a maximum flow rate of 3000 m3/h (273.15 K, 101325 Pa). The bundle consists of 30 30 stainless steel tubes, with two columns of half-tubes at both lateral plates. An additional bundle of 20 tubes is placed upstream the test section to regulate the inlet flow direction. The tubes have an outer diameter D = 30 mm, a thickness of 0.4 mm and are arranged in a rotated triangular pattern with a pitch ratio of 1.44 and an aspect ratio of 10.

1.2 Rigid configuration

For the fully rigid configuration, 6 tests listed in Table 1 have been carried out to measure the fluid forces (in the lift and drag directions). These forces are measured directly on an instrumented tube. A Fourier transform of the fluid forces (done with the *pwelch* function from Matlab) yields the power spectral densities (PSD). To measure local quantities, a bi-optical probe was introduced, its tip of the probe is positioned in the middle of a canal with an uncertainty on the lateral position estimated to $\pm$ 0.5 mm.

Table 1: Properties of rigid configuration tests

Test	Q_w (l/s)	Q_a (Nm³/h)	J_w (m/s)	J_a (m/s)	Corrected void fraction (%)	Time length of force signals (s)	Sampling frequency (Hz)	Downstream pressure (bar)
1	10.1	24.3	0.49	0.33	40.2	600	512	0.466
2	10.1	54.6	0.49	0.74	60.2	600	512	0.443
3	10.1	145.7	0.49	1.97	80.1	600	512	0.3932
4	9.9	321.9	0.48	4.35	90.1	600	512	0.3397
5	8.1	262.8	0.39	3.55	90.1	600	512	0.3504
6	6.6	214.5	0.32	2.90	90.1	600	512	0.3623

1.3 Flexible configurations

In this experimental study, two flexible configurations were tested, shown in Figure 2:

- Configuration n°11: 2 flexible tubes in the center of the bundle,
- Configuration n°3: a pattern of 7 flexible tubes in the center of the bundle.

The flexible tubes (identified by a number, as shown in Figure 2) are mounted on a single flexible stainless-steel blade (volume mass density of 7800 kg/m^3, Young modulus of 2.1 10^{11} Pa and Poisson's ratio of 0.3) of 100 (length)×25 (width)×4 (thickness) mm, instrumented with a strain gauge at the root, see Figure 3. For the configuration n°11 the averaged natural frequency in air of the moving tubes is 14.18 Hz and the averaged damping ratio is 0.045%. For configuration n°3, these values are respectively 31.96 Hz and 0.047%. The two configurations were subjected to increasing mass flow rates until the vibration amplitude was sufficiently high to indicate fluid-elastic instability. During a given set of test, the homogeneous void fraction was kept constant. Configuration n°11 (resp. n°3) was tested for an homogeneous void fraction of 40% (resp. 60%), results in terms of vibration are plotted in Figure 3.

For further details, please refer to the experimental deliverable of TITAN: https://go-viking.eu/images/resources/GO_VIKING_D4_5_titan_experiment__presentation_of_the_data_v2.pdf.

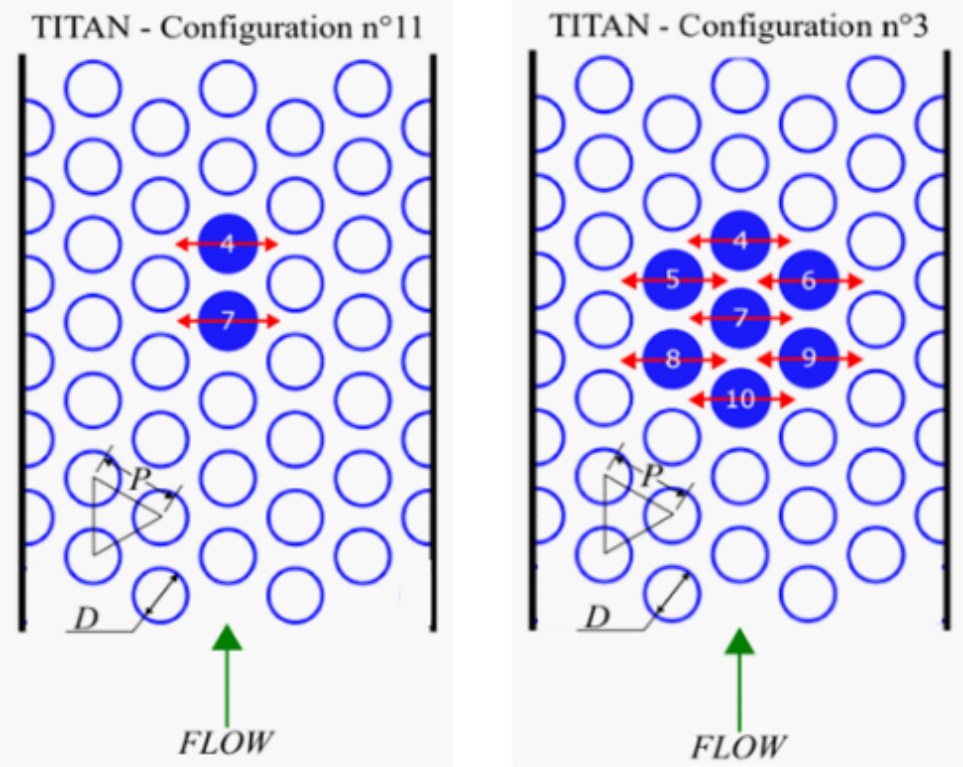

Figure 2: Sketch of the two flexible configurations with 2 and 7 flexibles tubes.

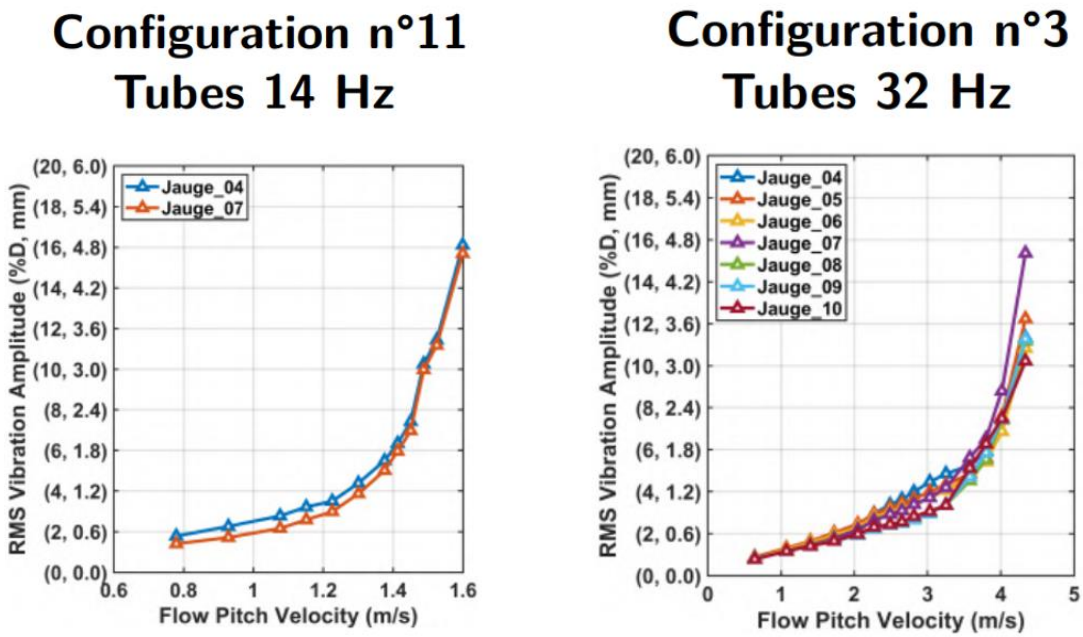

Figure 3: Experimental results of two-phase flow-induced vibration in TITAN. RMS vibration is presented with two different units : %D corresponding to the ratio between displacement and tube diameter and in mm.

2. Numerical modeling

2.1 EDF R&D

The neptune_cfd code is designed to model 3D multiphase flows using the two-fluid model of Ishii (1975) extended to n-phases, and the one-pressure approach of Delhaye et al. (1981). A set of balance equations for mass, momentum, and energy is derived by phase ensemble averaging, solved for each phase using an Eulerian-Eulerian approach, and coupled through inter-phase transfer terms. The density, viscosity, velocity, and volume fraction are defined for each field, in each cell of the domain. The work carried out for this study is limited to adiabatic cases and exclusively concentrates on liquid-gas flows, simplifying the system to the mass and momentum balance equations for each phase.

The definition of interfacial momentum transfers for each phase depends on whether the fields are continuous or dispersed. This interfacial momentum exchange term must be modeled to close the set of equations. Various approaches are available, depending on the specific two-phase flow regime. For bubbly flow, a dispersed approach is more appropriate for the gas field. However, in the case of slug flow, a large interface approach appears to be a better fit. To address multi-regime flows, where both small and large bubbles coexist like in the present application, the Generalized Large Interface Model (GLIM) was implemented in neptune_cfd.

The GLIM was developed to effectively model multi-regime two-phase flows by combining the features of the Large Interface Model (LIM) and the dispersed bubbly flow model. In the large interface approach, large interfaces are tracked using the volume fraction gradient and resolved, while the dispersed approach is used for smaller bubbles and consists of modeling bubble forces. For further details on the description of dispersed, large interface, and generalized large interface models, refer to Merigoux (2022).

Large gas bubbles in two-phase flows may not exhibit developed turbulence. Due to the complexity and computational expense associated with modeling turbulence, the assumption was made that the large bubbles exhibit no turbulence. However, the Rij-SSG model was used to account for the turbulence in the liquid phase. This model allows the use of a coarser mesh than the Rij-EBRSM, which requires a $y+ < 1$. Thus, the choice of the Rij-SSG model was a compromise between accuracy and computational efficiency, especially since we mainly focused on liquid-gas interfaces, and a very wall-refined mesh was not necessary. Ultimately, turbulent dispersion resulting from bubbles is considered in the dispersed phase.

The GLIM associated with a Rij-SSG turbulent model is used to simulate each test. The simulation is fully unsteady, it uses an adaptative time step to keep the CFL condition under 1 for each phase. The simulation is initialized with water at rest. At the inlet, gas, and liquid mass flow rates, hydraulic diameter, and bubble diameter of 1 mm are provided. At the outlet, a pressure condition is imposed. A wall-law is used for walls and y+ is kept over 30 and below 150. Void fraction distribution and force on the instrumented cylinder are post-treated to intercorrelate these variables.

2.2 NRG PALLAS

To model the two-phase flow, the single-pressure isothermal two-fluid model (TFM) is used. For this purpose, we use the multiphaseEuler solver of OpenFOAM 12. For each phase, a set of balance equations is solved for averaged mass, momentum. Regarding turbulence, closures are also solved to model it.. When it comes to studying two-phase fluid-structure Interaction (FSI), the classical TFM's fundamental limitation is that it averages out subgrid-scale two-phase structures, making it unsuitable for predicting dynamic stress fluctuations on solid surfaces in two-phase (FSI) problems. To overcome this, a hybrid approach is used to blend the classical TFM sub-grid closures (like drag and lift) with VOF-like 'tie-together' closures, using a blending function based on the local volume fraction. This way, the solver can shift between treating a phase as dispersed and applying a fully resolved interface treatment (VOF-like) with surface tension, where necessary. For the classical TFM, the Ishii and Zuber drag [17], the Tomiyama lift [18], Antal's wall lubrication [19], and Burns' turbulent dispersion model [20] are used. The LogMoM model is used to describe the unresolved bubble (droplet) size distribution [21].

To model the FSI, we use OpenFOAM's SixDoFRigidBodyMotionSolver, which treats the obstacle's translational motion as a simple mass-spring-damper system according to Newton's second law. Using interpolation, a net force acting on the surface of the obstacle is calculated from the total stress tensor. The motion of the obstacle in streamwise and centerline direction, as well as any rotation, is constrained, meaning that the obstacle can only move in lift direction (i.e., orthogonal to both the obstacle's centerline and streamwise direction). The original 6-DoF FSI solver in OpenFOAM is limited to single-field solvers because hard-coded parameters restrict fluid force computations to single-phase flows. To overcome this limitation, a new solver has been developed that is compatible with the multiphaseEuler solver.

In OpenFOAM, the mesh motion method is based on an Arbitrary Lagrangian-Eulerian (ALE) formulation. The introduction of the PIMPLE algorithm in OpenFOAM enables the use of outer corrector loops to ensure the convergence of pressure and velocity. As a result, the mesh update function is incorporated within the PIMPLE outer corrector loop. In OpenFOAM's FSI coupling approach, the following steps are executed at each time step. First, fluid variables (velocity and pressure, void fraction, etc.) are initialized using the solution from the previous step. Simultaneously, if the rigid body has moved, the mesh is updated accordingly. Next, through an inner PISO cycle, the flow fields are updated to ensure mass conservation. Finally, the hydrodynamic force and moment on the rigid body are calculated via surface integrals. For TITAN simulations, we used one outer corrector, making the FSI coupling approach an explicit method.

2.3 EDF UK

EDF UK R&D conducted simulations for three cases of the rigid configurations: **T1**, **T2** and **T3** (see Table 1). All 3D computations were conducted in the SIEMENS StarCCM+ v25.006 finite volume CFD solver. The focus was on assessing the best approaches in simulating bubbly and slug flows in StarCCM+.

The method selected for assessment for the TITAN case was the Volume of Fluid (VOF) [7] method. The Eulerian Multiphase Method (EMP) [8]was also tested.

VOF simulates flows of fluids that are immiscible with the assumption that the numerical grids are capable of resolving the interface between the fluid phases in the flow. There is a phase indicating function which determines the volume fraction occupied by one of the phases. If the phase is present in a numerical cell, this function is defined to have the value of 1, but zero otherwise. In StarCCM+, the VOF method is combined with the HRIC blending scheme for reconstructing the interface density and maintaining a sharp interface between the phases. A user can specify the Sharpening Interface Factor, which ranges from 0.0 to 1.0. A Sharpening Factor of 0.0 indicates that there is no reduction in numerical diffusion. On the other hand, a factor of 1.0 leads to no numerical diffusion and a very sharp interface for simulation; this setting is unstable. For the TITAN cases, a Sharpening Factor of 0.9 was specified to accurately and stably capture the interface and prevent numerical diffusion.

There is a collection of models that predict the influence of the interaction between the water and air phases for the VOF method. The interaction models selected were:

- Interaction Area Density Model: The interaction area density quantifies the interfacial surface area per unit volume between phases, which is essential for calculating interphase momentum transfer in VOF simulations. In StarCCM+, this parameter affects the accuracy of interface tracking and the calculation of interfacial forces. For air-water flows in tube bundles, proper specification of interaction area density ensures correct representation of drag forces and turbulent momentum transfer across phase interfaces, particularly important in bubbly flow regimes where interfacial area significantly influences the flow dynamics.

- Interface Turbulence Damping Model: The Interface Turbulence Damping model accounts for the suppression of turbulence near phase interfaces, a phenomenon observed in multiphase flows where large gradients, due to a relatively high velocity between the water and air phases, inhibit turbulent fluctuations perpendicular to the interface [9]. This option modifies the behaviour of the turbulence model in interfacial regions, preventing unrealistic turbulence production.

- Surface Tension Force Model: The Surface Tension Force model uses the continuum surface force (CSF) approach to compute the capillary forces at the interface of the phases [10]. The simulations used the semi-implicit surface tension approach to improve numerical stability in the computations by reducing the effect of parasitic currents or spurious velocity. The semi-implicit way of treating the surface tension force term in the formulations allows for larger time steps while maintaining accuracy in capturing interface curvature effects.

For the three cases, the continuous – disperse topology was used. Water was specified as the continuous phase while air was indicated as the disperse phase. Constant density was specified for the two phases. Turbulence modelling is handled using the two-equation *k-ω SST* method with the All y^+ wall function routine. Mixture turbulence is used to represent the two phases together.

Pressure-velocity coupling was handled with the SIMPLEC method. Spatial, turbulence, temporal and volume fraction convection were discretised as 2nd order. An adaptable time step was used with the maximum CFL number stipulated as o.75.

A homogeneous mixture of the air and water phases was stipulated at the inlet boundary. The computational domain upstream of the tube bundle was made to be long enough (10*D*) to allow sufficient interaction of inertia, gravity, shear, and surface tension effects, leading to the development of the flow and volume fraction profiles upstream of the bundle.

2.4 ASNR

Ansys Fluent v2024 R1/R2 was employed. Two all-flow-regimes approaches are implemented inside Fluent: the Algebraic Interfacial Area Density (AIAD) model and the GEneralized TwO Phase flow (GENTOP) model. AIAD is a two-fluid model, the first version of which was proposed [12,13] and a second version with improved blending functions was later proposed [14]. GENTOP is a three-field model described in Hansh et al. [15]. A k-ω SST turbulent model is used for each phase.

ASNR initially intended to employ the GENTOP model to simulate TITAN. However, the poor numerical stability of this model inside Fluent prevented from running successful simulations. GENTOP was therefore abandoned and the AIAD was instead retained, which showed higher (even if still tricky) numerical stability.

Simulations were first run on 2D meshes to study different numerical and physical set-ups. 3D simulations were then run on a mesh featuring a tube length equal to 3 times the tube diameter (which represents a smaller section compared to the actual tube length equal to 10 times the tube diameter).

A 7-class population balance was used to estimate bubble diameter for 2D simulations. Unfortunately, the activation of the same model made the code crash when run in 3D: 3D simulations were run with constant bubble diameter, corresponding to the average bubble diameter expected (4.10^{-3} m). It has to be noted that 2D simulations that were run with population balance and with constant bubble diameter showed a limited difference in the calculated force spectrum.

Constant (in space and time) velocities and void fraction were imposed at the inlet boundary condition. Symmetry boundary conditions were imposed on the two faces in the spanwise direction (domain width) for the 3D simulations. A pressure drop was imposed inside the cells close to the outlet boundary condition, in order to limit high flow recirculation that would otherwise develop and influence the flow inside the tube bundle region.

The main limitation encountered was the impossibility of running simulations with space discretization scheme of order higher than first order upwind, because of numerical instability of higher order schemes. Another important detail to note is that the only possible option provided by Fluent when using the AIAD is to use the “Compressive” scheme [16] for the volume fraction transport equation.

2.5 Sum-up of the numerical approaches

Table 2: Sum-up of the numerical approaches from each partner

Partner	Software	Two-phase modeling	Turbulence model	Type of Inlet	Type of Outlet
EDF R&D	Neptune_cfd	Euler-Euler with Generalized Large Interface model	Rij-SSG with wall-law	Homogeneous	Averaged pressure condition
NRG	OpenFOAM 12 (Foundation branch)	Hybrid two-fluid model (HZDR model)	K-Omega SST for liquid phase and K-Omega SST Sato for gas phase	Uniform velocities and volume fractions are set based on the experimental superficial velocities and volume fractions	Fixed pressure, zero-gradient for k and Omega, Void fraction, pressureInletOutletVelocity for velocity,
ASNR	Fluent v2024	Euler-Euler AIAD	k-w SST – per phase	Homogeneous	Fixed pressure
EDF UK	StarCCM+	Volume of Fluid (VOF) Method	k-w SST	Homogeneous	Pressure

3. Calculation domain & Mesh

3.1 EDF R&D

The calculation domain is based on the tube bundle geometry, the length of the cylinders is reduced to 2 diameters (2D) with a periodicity condition, however some short tests were done with 10D in order to verify the consideration of all relevant phenomena. The domain is extruded 10D upstream and downstream of the tube bundle, resulting in a mesh composed of 8 million conformed hexahedron cells (respectively 40 millions with 10D). Views of the domain and the mesh are presented in Figure 4. A sensitivity to the domain size was performed and discussed in the following part.

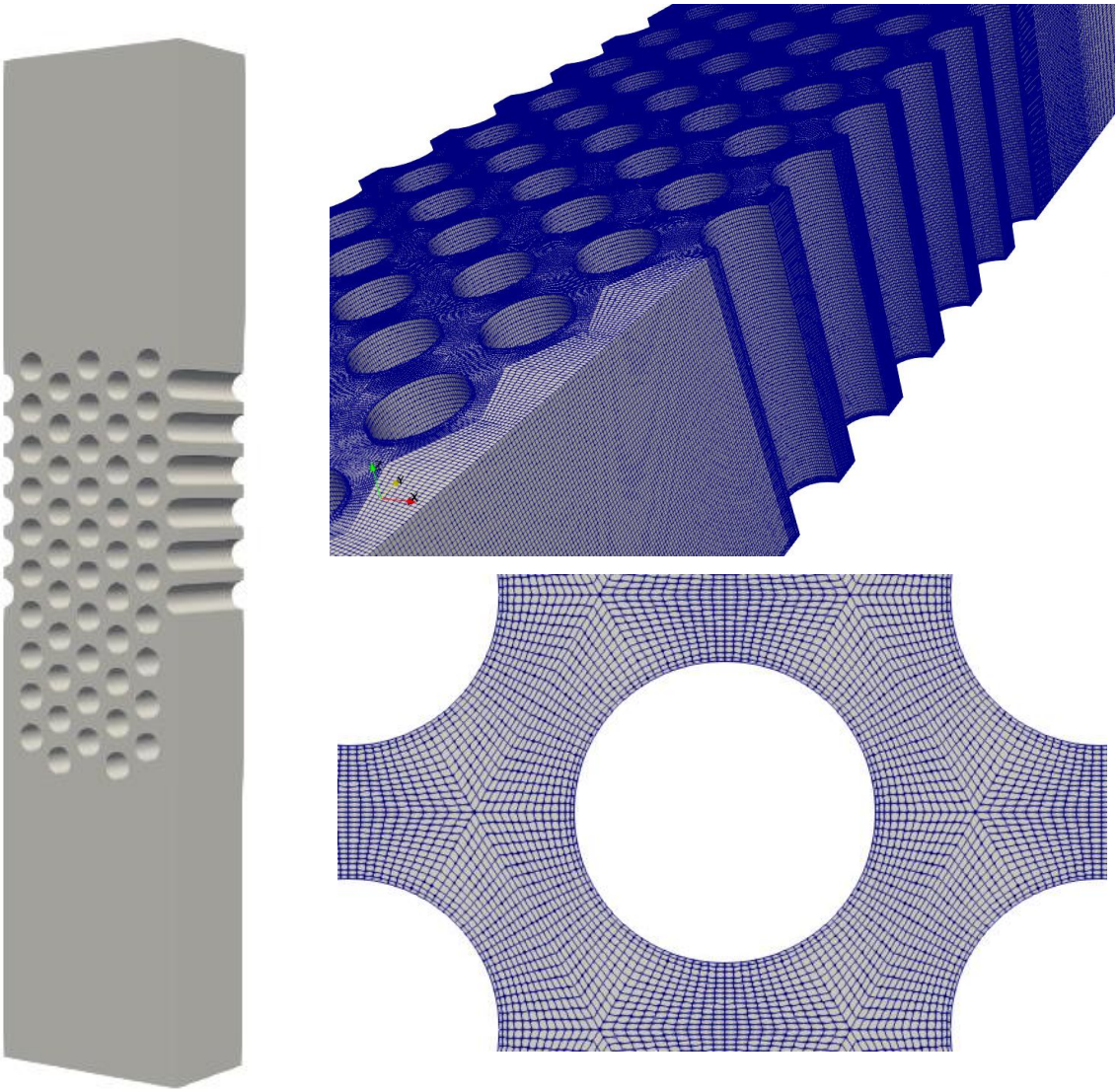

Figure 4: Calculation domain and view of the mesh from EDF R&D.

3.2 NRG PALLAS

The whole bundle is modelled. The domain inlet boundary is located 1897 mm from the first tube in the bundle (distance from the edge), upstream of the tube bundle. The outlet patch is located 620.2 mm from the last row of the bundle (distance from the edge) downstream of the tube bundle. The total size of the domain is $\delta x \times \delta y \times \delta z = 224.47\ \mathrm{mm} \times 2959.2\ \mathrm{mm} \times 300\ \mathrm{mm}$. The minimum mesh size is 2 mm. Prism layers are considered at the channel walls and around the tubes. The resulting mesh has a total of 1 M cells and is presented in Figure 5.

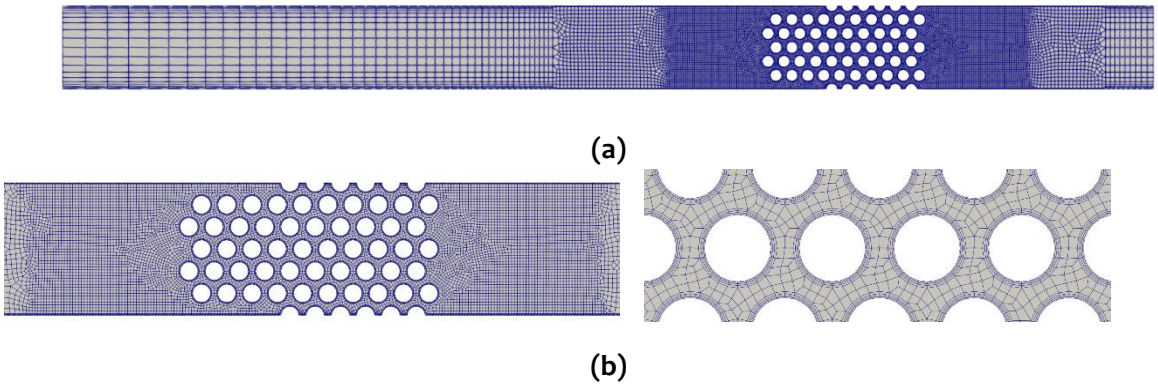

Figure 5: cross sections of the computational domain. (a) Full domain in the x-y plane. (b) Left: mesh in the vicinity of the tube bundle.

3.3 ASNR

The numerical domain vertically begins at the position where the mixing plate is placed upstream of the tube bundle. The outlet boundary condition is placed 0.5m downstream of the last row of the bundle.

The mesh is conformal and fully hexahedral and was built with ICEM CFD. The wall refinement was set to allow a value of y+ close to 1 on the tubes. The maximum cell size in the bulk (of the tube bundle region) is 1.7mm. Details of the mesh are provided in Figure 6. The vertical cell size in the regions upstream and downstream of the tube bundle was larger than inside the bundle region. Mesh sensitivity was studied in 2D employing a mesh refined by 20% in all directions (resulting in a maximum cell size of 1.3mm in the tube bundle region) and show no significant variation in the calculated force spectra.

The 3D mesh was built by extruding the 2D mesh along the spanwise direction. Constant layers of 2.0mm were used (see Figure 6) for a total of 4.1 millions of cells.

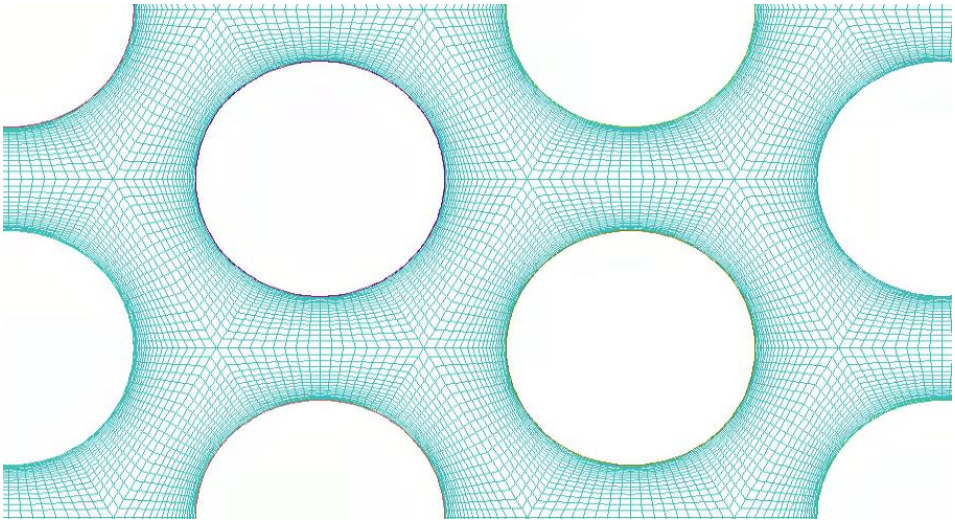

Figure 6 VIew of the mesh in the tube bundle used by ASNR.

3.4 EDF UK

The computational domain of the 50 staggered tube bundle was modelled as fully 3D; the entire width of 10D was simulated to match the experiment (see Figure 7). The Trimmed Mesh method in StarCCM+ was used to generate mostly hexahedral grids with minimal cell skewness. The base size for the mesh generator was 3 mm. A prism section to represent the boundary layer was defined with two cells, the width of the prism section being 17% of the stipulated base size. Also, the domain is extended upstream and downstream of the tube bundle by 10D. Hence, the resulting total grid size of the mesh used for the T1, T2 and T3 cases was 5.8 million cells. The mean y+ of the tubes in the domain had a range of $3 - 14$. To capture the smallest scales and bubble sizes that were not sufficiently reduced by the grid, the Adaptive Mesh Refinement (AMR) option was activated during the simulation. However, AMR was limited to only one refinement level to limit the overall grid size.

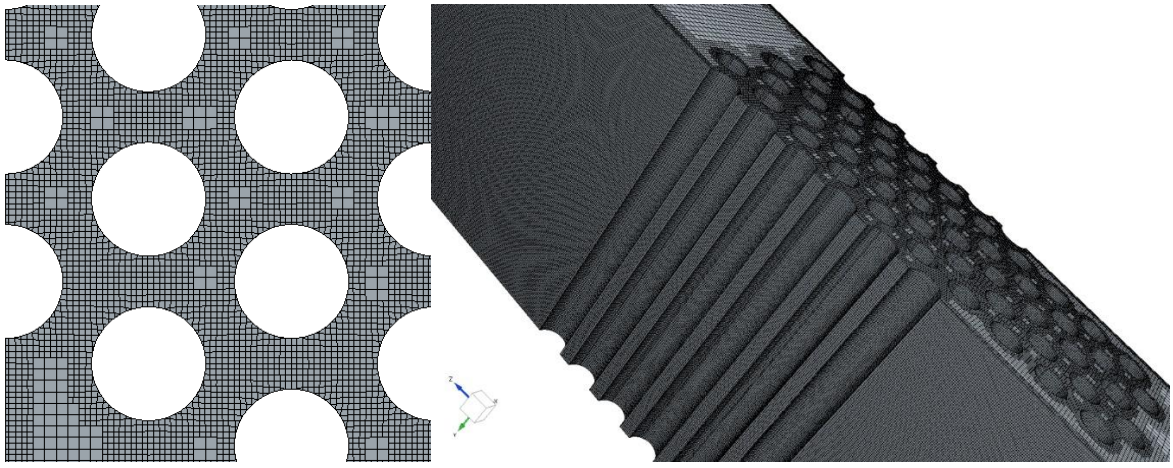

Figure 7: Zoomed-in sections of the computational grid used for the TITAN cases.

3.5 Sum-up of the calculation domains & Mesh

Table 3 Sum up of the calculation domains & mesh from each partner

	2D or 3D	Tube Length	With upstream tube bundle	periodicity	Type of mesh	Total number of cells	Dr (mm) at cylinder wall	Dx_mean (mm)
EDF R&D	3D	2D and 10D	0.3 m	Yes (2D) and No (10D)	Hexahedral	8M (2D) 40M (10D)	$5\ 10^{-4}$ m	
NRG	3D	10D	1.89 m	no	Unstructured hexagonal	1 M	0.3 mm	3 mm
ASNR	3D	3*D	0.416 m	Symmetry	Hexa	4.1M	$1.5 \cdot 10^{-4}$m	
EDF UK	3D	10D	0.3 m	No (10D)	Hexahedral - unstructured	5.8 M	0.25	1.5 – 3.0

4. Rigid configuration

4.1 Qualitative analysis of the flow through numerical simulation

For the present numerical benchmark, the choice has been made to compare simulations results of Case 2, which is a slug to churn flow pattern. In Figure 8 instantaneous void fraction distributions obtained by the different partners across the triangular tube bundle of TITAN experiment are shown. These distributions highlight discrepancies in terms of behavior of the two-phase flow, related to the choice made by partners in terms of model and calculation domain especially. EDF UK, EDF R&D and ASNR distributions show a dispersed flow with a void fraction between 25 and 35% where some large gas structures (size similar to the gap) at 100% of void fraction are present. On the other hand, the NRG PALLAS simulation highlights larger structures not limited to the gap size.

In Figure 9 the time-averaged void distribution across the tube bundle is presented for Case 2 from the simulation of each partner. The NRG PALLAS simulation highlights a liquid layer at the front of the cylinder with an heterogeneous distribution of void along the width. On the other hand, EDF UK, EDF R&D and ASNR highlight a homogeneous distribution of void around 40% with a liquid layer at the tube rears (rear tube wall (downstream direction)) with some discrepancy in terms of thickness (between 25% and 50% of the gap). The predicted value is also in agreement with the experiment since this case has a homogenous void fraction of 39.8% with a slip velocity between phases probably close to one due to the higher superficial liquid velocity.

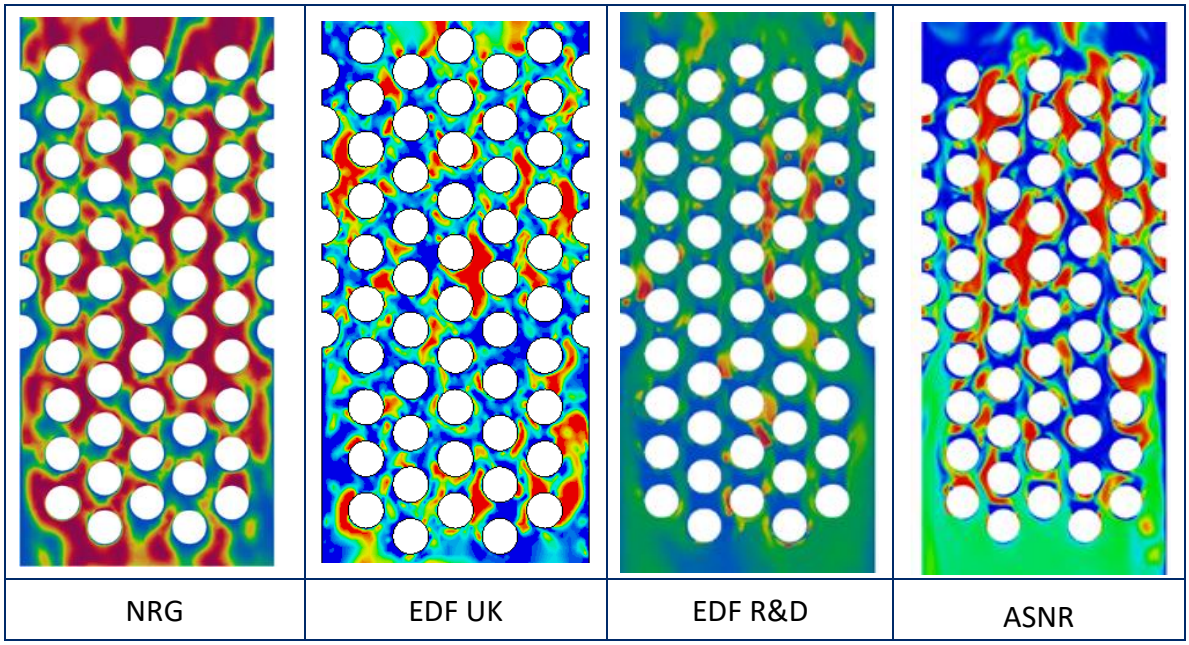

NRG	EDF UK	EDF R&D	ASNR

Figure 8 Instantaneous void distribution along the tube bundle for Case 2 from each partner (from 0% (blue) to 100% (red)).

Considering the discrepancy in terms of numerical models and calculation domains, having such quantitative similarities between simulations strengthens confidence in the numerical predictions.

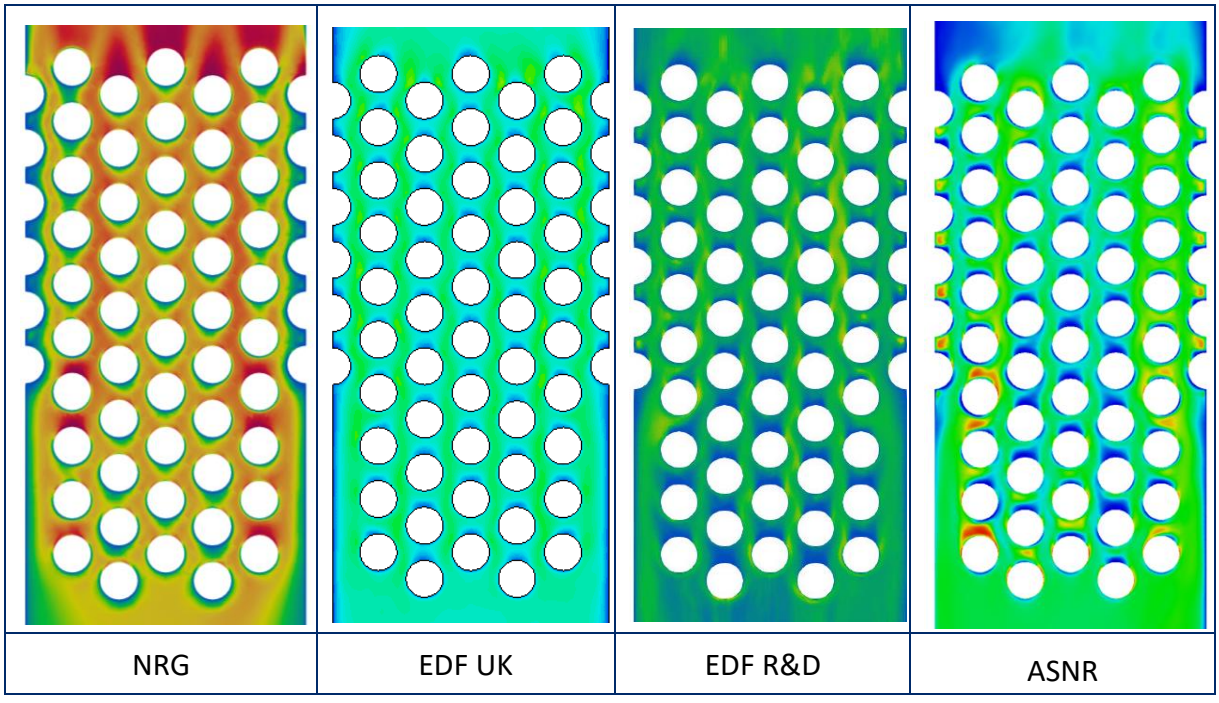

NRG	EDF UK	EDF R&D	ASNR

Figure 9 Averaged void distribution along the tube bundle for Case 2 from each partner (from 0% (blue) to 100% (red)).

4.1.1 Qualitative analysis from EDF R&D

In Figure 10, a preliminary sensitivity study on the length of the cylinder from 1D with periodicity to 4D with periodicity for the Case 1 to evaluate the effect on the force spectra, was performed and highlighted that after 2D length the force prediction are very similar. Then, a 10D length simulations of the different cases to see the variation of void distribution along tubes, showed that even for high void fraction cases a homogeneous distribution (see b) and c)). Thus, the choice was to perform the simulation on the 2D length with periodicity to have a longer force signal to plot the force probability density functions. Moreover, a sensitivity to the mesh refinement and to the inlet bubble diameter was performed (since the inlet two-phase characterization was not available) on Case 1, which was the most sensitive to the inlet characterization.

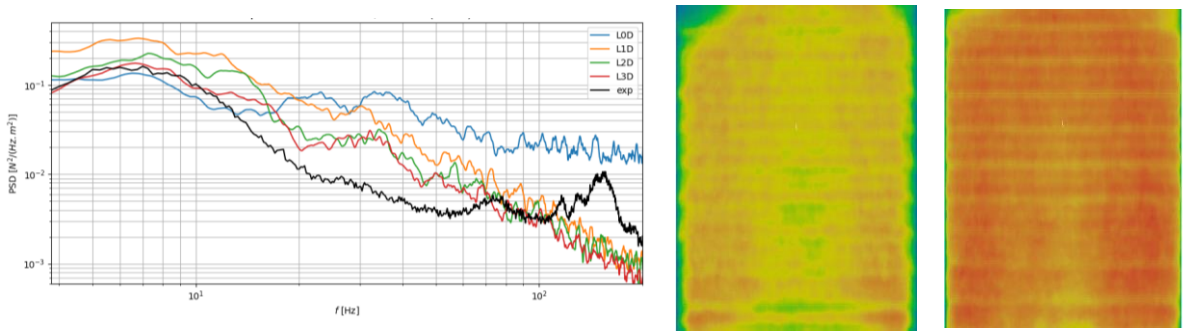

a) b) c)

Figure 10 Sensitivity analysis on preliminary computations to the reduced length with periodicity on Case 1 on force spectra (a), averaged void distribution with the full domain along tubes for Case 3 (b) and Case 4 (c)

In Figure 11, instantaneous and time-averaged void distributions along the tube bundle are presented and show discrepancies related to the flow patterns in agreement with the observed flow pattern from the experiment.

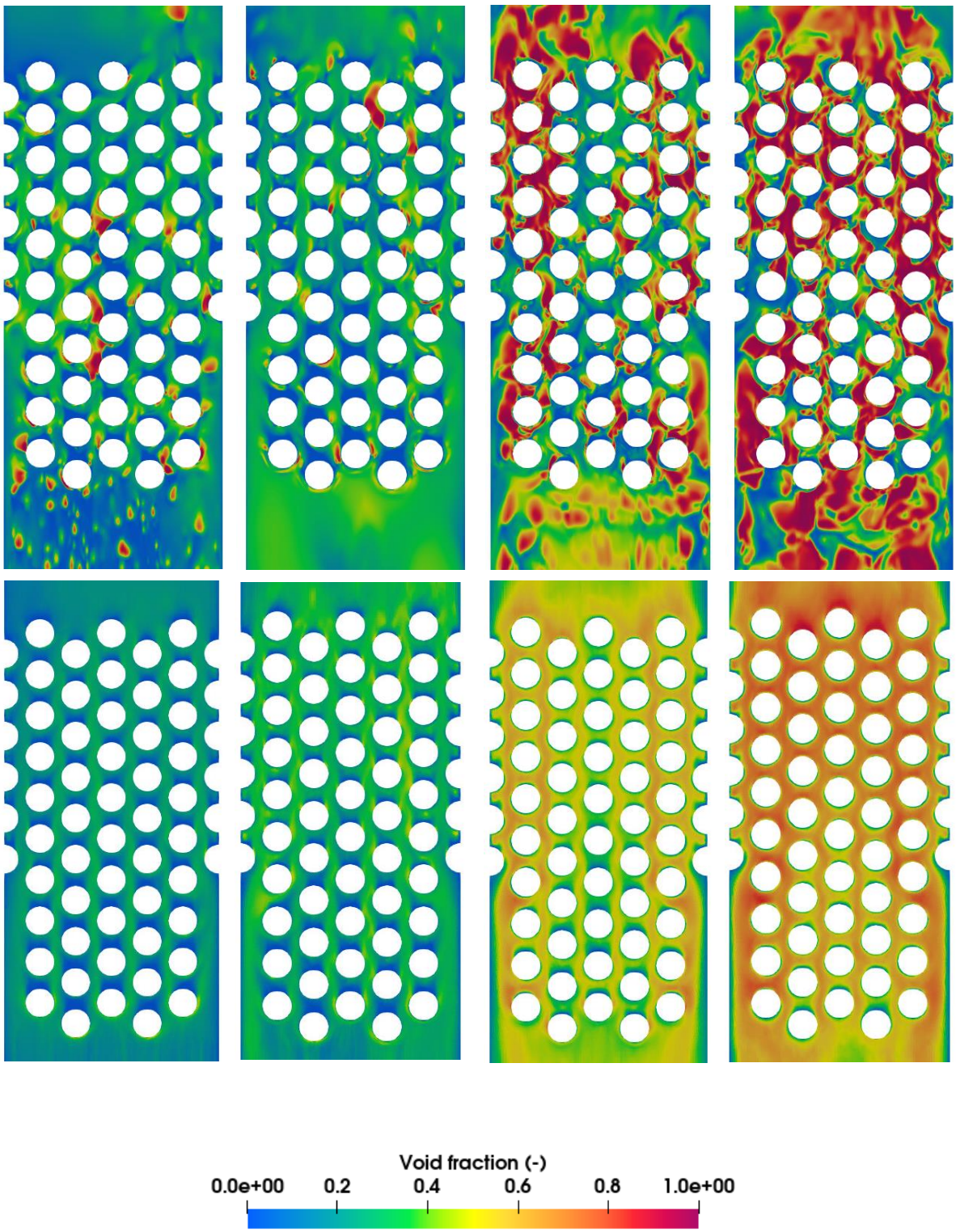

Figure 11: Instantaneous (top) and averaged (bottom) void fraction distribution along the tube bundle from EDF R&D.

Funded by
the European Union

4.2 Void fraction: Numerical vs Experimental results

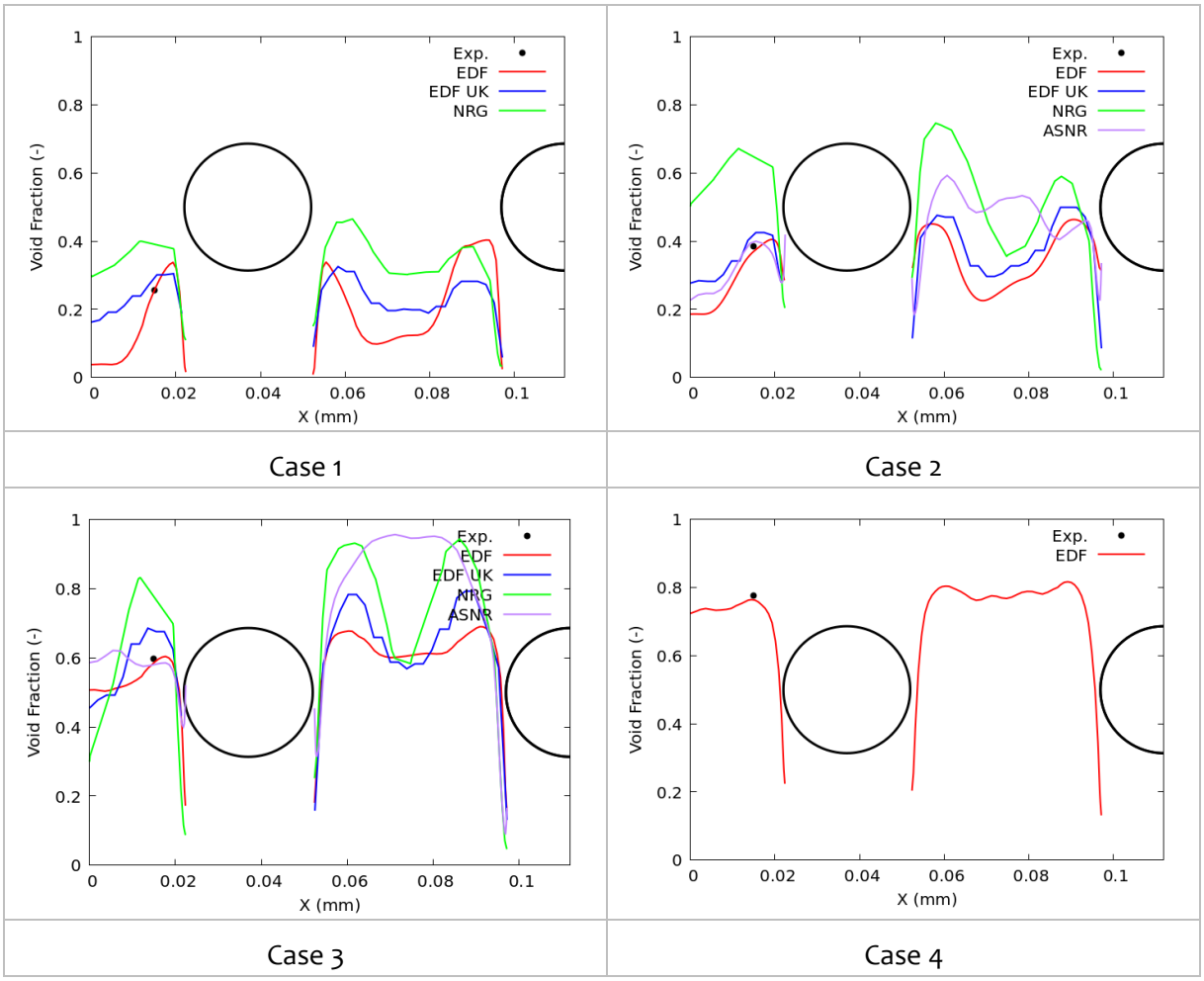

Figure 12 Void fraction profile along x at the optical probal altitude from each partner for each case.

A comparison was then performed in terms of void fraction across the tube bundle at the height of the optical probe for each case simulated by the partners, see Figure 12. For Case 2, for which the void distributions are shown in Section 4.1, a reasonable agreement between EDF UK, EDF R&D and ASNR simulation at the location of the optical probe, and more generally across the tube bundle, can be seen. For Case 1 and 3, this is also true for EDF UK and EDF R&D simulations highlighting similarities in terms of two-phase flow predictions between the different numerical models. However, due to the lack of two-phase measurements (like void or velocities) in TITAN, the present comparison is the only one possible with the experiment in terms of flow.

4.3 Fluid forces: Numerical vs Experimental results

Regarding fluid forces, lift and drag Power Spectral Densities (PSD) from the experiment are available for each case. In Figure 13, force spectra from Case 1 to Case 4 are presented with the numerical results from each partner.

NRG PALLAS results appear to be over-estimated in terms of force predictions in the different cases. Similarities observed between EDF R&D, EDF UK and ASNR with three different codes and set-ups are also confirmed by the force prediction where there is a correct agreement between simulations and experiment for the different flow patterns, especially for Case 2 and 3 (and 4 for EDF) for which the agreement is excellent.

This is less true for Case 1, being a bubbly to slug flow. This is probably due to the numerical approaches to perform the simulations. Here, the resolved gas structures (with VOF or GLIM (where the LIM is the resolved part of the model) approaches) are responsible of the main force fluctuations whereas for the dispersed phase, the RANS approach is used, consequently the force fluctuations are not well represented without a proper refinement for small structures. As partners worked first on Case 2, the mesh should probably be more refined in order to resolve more gas structures, thus having a better prediction of force fluctuations. This was done by EDF in an inlet gas distribution and mesh sensitivity analysis from which it was found that the inlet bubble diameter should be at least 5 mm in order to have the correct force profile. For other cases, the sensitivity to the inlet gas distribution appeared to be much lower, probably due to the high gas flow rates leading to high coalescence and large gas structures.

The triangular arrangement coupled to a slip between phases close to 1 are probably responsible for the stability of the flow and the agreement between simulation, since the flow is more restricted by the geometry than in a square arrangement. Thus, having a different inlet gas size distribution than the experiment appears to be less predominant after a couple of rows in the tube bundle than for the square arrangement. This finding is of great interest since there is no information on the gas size distribution from the experiment at the inlet except the flow rates. Consequently, with 3 different numerical models and inlet conditions, having such similar results is even more surpising.

Finally, the present result shows for different homogenous void fraction and mass flow rates a correct agreement from three different partner contributions with the experiment in terms of void fraction and force prediction. Thus, this speaks well for the fluid-structure interaction simulations where different flow rates will be simulated, since there is no correspondance between rigid and flexible inlet conditions.

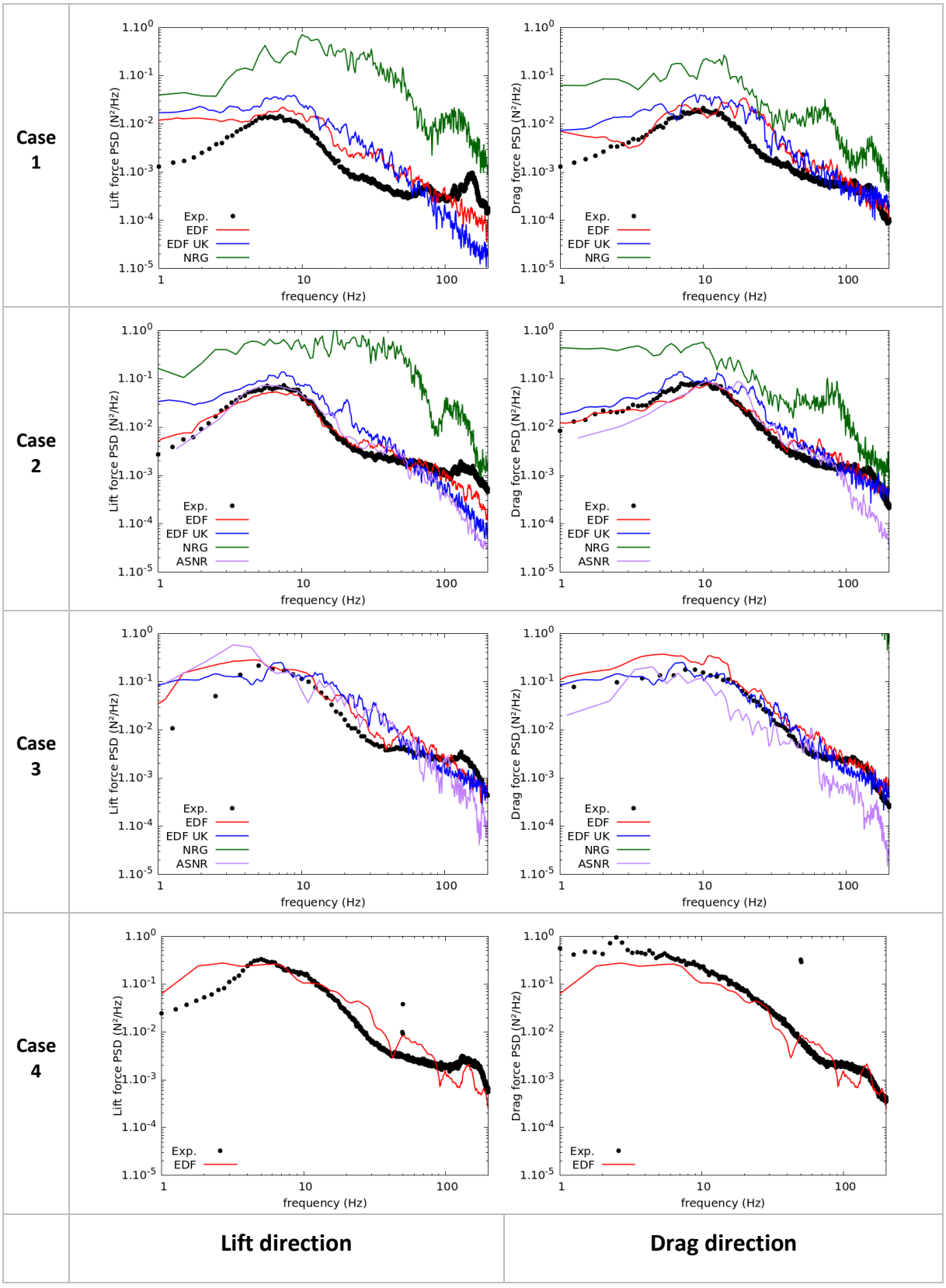

Figure 13 Cross comparison of PSD force spectra for drag and lift direction for each case.

5. Flexible configuration

5.1 EDF R&D contribution

A missing feature in neptune_cfd was the Arbitrary Lagrangian–Eulerian (ALE) framework, already available in code_saturne for fluid–structure interaction (FSI) applications. This mesh-deformation method complements the existing Immersed Boundaries (IBM) approach, offering improved computation of the boundary layer. In several configurations, ALE proves to be a more appropriate choice, except for significant displacement (large mesh deformation or contact between tubes). Thus, the functionality was developed for the need of GO-VIKING within neptune_cfd with the same FSI coupling developed in code_saturne (iterative coupling).

For the present case, the configuration n°11 with two-flexible cylinders for a homogeneous void fraction of 40% and a pitch velocity of 0.78 m/s is simulated. Based on the information from the experiment and according to the modal theory of a cantilever beam in mode 1, the modal mass at the tip is 0.409 kg for the considered geometry. The measured frequency is 14.18 Hz, which gives an angular frequency ω = 89.1 rad/s. The measured damping is ζ = 0.00045. Consequently, based on the modal theory at the tip, the parameters to be considered are as follows: m = 0.409 kg, k = 3245 N/m and c = 0.033 N·s/m. The fluid forces originate from a section of length 2D; therefore, the coupling model is adapted to account for the reduced excitation length.

The original set-up with a 2D-length was used. A free-rigid body motion is allowed for the 2 cylinders of interest. Their motion is computed with an iterative implicit coupling following a Newmark algorithm with δ = 0.5, β = 0.25 meaning no numerical damping introduced and a second order unconditionally stable resolution.

Results obtained for the present case are presented in Figure 14.

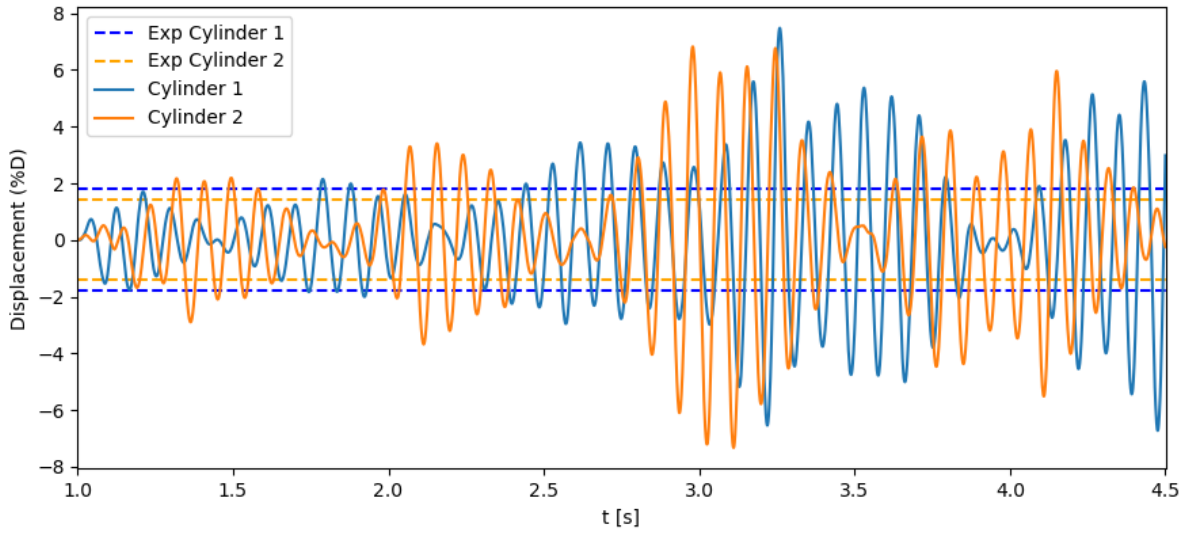

Figure 14 Displacement in %D of each cylinder from the simulation compared to the RMS displacement from the experiment for configuration n°11.

The time of computation is too low to be converged in terms of RMS of displacement, however the numerical prediction over 3.5s of vibration are:2.27 %D for cylinder 1 and 2.22%D for cylinder 2, while the experimental RMS are 1.78%D and 1.42%, respectively. The present results are thus preliminary and need further investigation, but are promising, nonetheless. Four other higher pitch velocities were simulated in order to compare the obtained results to the experiment and to predict the critical velocity numerically. However, when tackling higher pitch velocities, the vibration amplitude is also higher. As an example, for a case with an RMS of 10%D experimentally, some peaks of amplitude appear at 18%D (5.4 mm) numerically, depending on the position of both cylinders. Using the ALE approach for the present mesh leads to a significant cell distortion, thus preventing the continuation of the simulation. In the present preliminary computation, the modal theory was applied at the tip, wwhile in the experiment contacts were probably observed, which is not possible to simulate with the present numerical model. Thus, for future simulations, we will propose to use the modal theory not at the tip, but at mid-span to allow simulation at higher pitch velocities.

5.2 ASNR contribution

The numerical simulations of case 2 and case 3 of the fixed configuration proved to calculate force spectra in good agreement with the experimental results. On the other hand, the flexible configuration experimental results were obtained for flow conditions (gas and liquid mass flow rates) significantly different from the fixed configuration: this means that a preliminary validation of the force spectra calculated with the flow conditions specific to the flexible configurations cannot be realized. This aspect somehow limits the interest in performing FSI simulations of the two flexible configurations: if discrepancies in the calculated vibration response compared to experimental values were observed, the source of such behavior could not be understood. For this reason, the coupled FSI simulations were run for the flow conditions of case 2 of the fixed configuration (for which the calculated force spectra were validated) but letting the two flexible tubes of configuration 11 vibrate.

The tubes are considered as rigid body, meaning that only purely translational motion is allowed in the lift direction. The rigid body equation consists of a one-degree-of-freedom mass-stiffness-damping equation. The equivalent rigid body mass and stiffness values were calculated based on a 3D FEM model of the real experimental flexible blade configuration. The damping coefficient was calculated based on the damping value measured experimentally and provided in the Titan report. The HHT algorithm was used to solve the structural motion with time. The model was previously developed and implemented inside Fluent through UDFs by [1].

A strong fluid-structure coupling was used. Two fluid-structure sub-iterations per time-step were imposed: almost no structure displacement variation was found between the first and the second sub-iteration, however the second sub-iteration was kept ensuring numerical stability of the coupling. An ALE approach was used to deform the mesh to accommodate the structure displacement.

The displacement as a function of time of the two vibrating tubes is presented in Figure 15 zoomed along a transient of 2 seconds. The two tubes show a very similar vibrational response in terms of frequency and amplitude. This can also be confirmed by the PSD of displacement signal, presented in Figure 16: both amplitude and frequency are almost identical between

the two tubes. The vibrating frequency is about 13.7 Hz, consistent with the natural frequency in air of 14.18 Hz. The RMS calculated from the displacement signal for tubes 7 and 4 are equal to 1.48% and 1.66% of the tube diameter, respectively. Even if these values cannot be directly compared with the corresponding experimental values (that are not available), flow conditions similar to case 2 of the fixed configuration (Jg=0.74m/s and Jl=0.49m/s) are found for case 3 of configuration 3 (Jg=0.77m/s and Jl=0.632m/s). For the latter, the experimental displacement rms ranges from 1.40% to 1.64% (depending on the tube) of the tube diameter: such values are very similar to the calculated displacement of the simulated case.

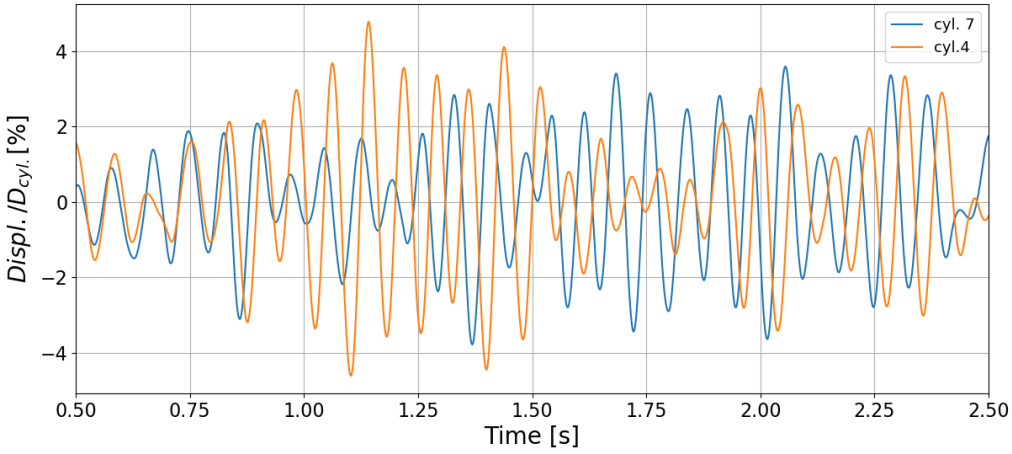

Figure 15 calculated displacement of tubes 4 and 7 (the tube numbering refers to configuration 11

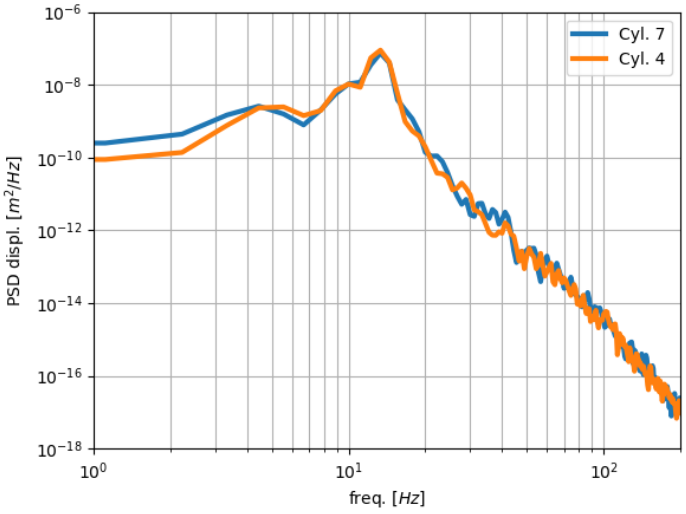

Figure 16 PSD of the calculated displacement of tubes 4 and 7 (the tube numbering refers to configuration 11).

5.3 NRG PALLAS Contribution

The flexible configurations were tested experimentally under gas and liquid mass flow rates that differed from those used for the fixed configuration. As a result, a preliminary validation of the force spectra computed specifically for the flexible configurations could not be performed. As also mentioned in section 5.2, this limitation reduces the value of conducting full Fluid-Structure Interaction (FSI) simulations for the two flexible configurations. Indeed, if discrepancies were observed between the calculated vibration responses and the experimental measurements, it would be difficult to identify the underlying cause.

For this reason, a preliminary coupled FSI simulation was performed using the flow conditions of Case 2 from the fixed configuration, for which the force spectra had already been successfully validated. Due to the constraints of the current numerical model (specifically, the rigid body motion solver in OpenFOAM), only one moving tube was considered in the simulation: the upper moving tube in Configuration 11.

Comparison of the flow-only simulation results with the experimental data revealed that the forces acting on the tube were significantly overestimated in terms of amplitude. A sensitivity analysis showed that this overestimation was caused by the two-phase structures captured on the mesh being excessively large. Further investigation indicated that the original mesh was too coarse, particularly in the upstream region of the tube bundle.

To improve the accuracy of the numerical results while keeping the computational cost acceptable, the prism layers were removed, the minimum bulk mesh size was reduced from 5 mm to 2.5 mm, and the length of the refinement region upstream of the bundle was increased by 50%. These mesh modifications led to a significant improvement in the agreement between the numerical and experimental force spectra for Test 2. This improvement is illustrated in 7, which compares the power spectral density (PSD) of the drag force (left) and lift force (right) obtained with the original mesh and the improved mesh. In the FSI simulation, therefore, the improved mesh is used.

For the flexible configuration, the moving tube is modeled as a single-degree-of-freedom mass-spring-damper system, governed by Newton's second law. Only translational motion in the lift direction (perpendicular to the incoming flow and the tube axis) is permitted, while movement in the streamwise direction, along the tube centerline, and all rotational degrees of freedom are completely restrained. The structural model includes a spring stiffness of 6857.14 N/m and a damping coefficient of 0.306 Ns/m. The effective mass of the tube is set to 0.864 kg.

The time history of the tube displacement, together with its power spectral density (PSD), is shown in 8. Figure 18: History of the tube displacement (left) and corresponding power spectral density (PSD) of the displacement (right). The root-mean-square (RMS) tube displacement is 0.9% of the tube diameter, with a dominant vibration frequency of approximately 20 Hz.The root mean square (RMS) displacement of the tube is 0.9% of the tube diameter, which corresponds to a relatively small vibration amplitude. The PSD of the displacement exhibits a clear peak at approximately 20 Hz, indicating that this is the dominant vibration frequency.

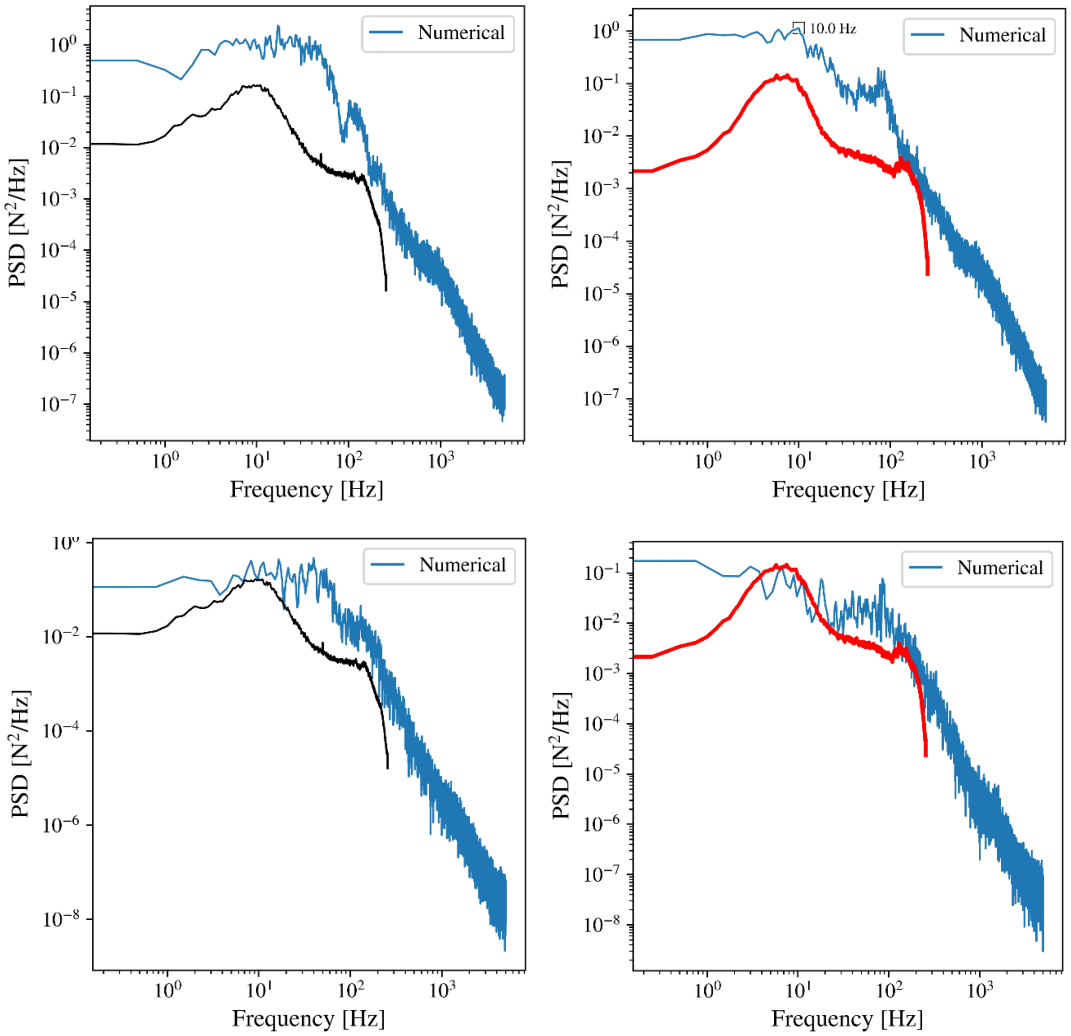

Figure 17: Power spectral density (PSD) of the drag force (left) and lift force (right) acting on the tube. Comparison between the results obtained with the original mesh (bottom) and the improved mesh (top) for Test 2.

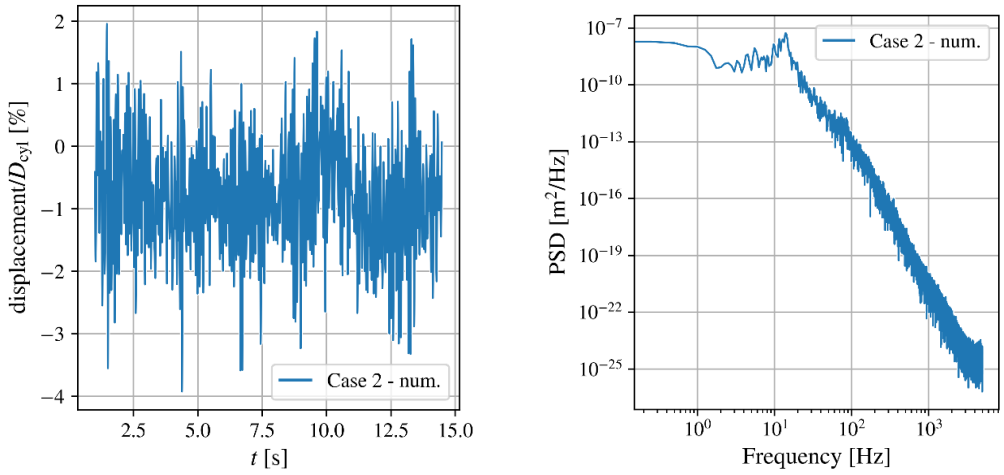

Figure 18: History of the tube displacement (left) and corresponding power spectral density (PSD) of the displacement (right). The root-mean-square (RMS) tube

displacement is 0.9% of the tube diameter, with a dominant vibration frequency of approximately 20 Hz.

5.4 EDF UK Contribution

The fluid–structure interaction simulations were performed using the two–way CFD–FEA coupling approach implemented in StarCCM+. StarCCM+ enforces two coupling options to conserve energy and momentum across the interface: the kinematic coupling condition, where the velocity of the fluid at the interface is matched with the velocity of the solid body; the dynamic coupling condition, where the forces at the interface between the solid and fluid domains are matched.

In the TITAN experimental setup, the tube ends meet the walls of the rig. In the simulations, to ensure that the fluid mesh does not become distorted by this setup during tube motion, the length of the vibrating cylinders was reduced by 5 mm at each end. This reduction created an offset between the vibrating tubes and the end walls, giving an effective length of 290 mm for the cylinders in motion.

The displacement of the vibrating cylinders is computed using the solid stress model in StarCCM+, which employs the finite element method to determine displacements and corresponding stresses and strains in the solid domain. Linear–elastic models were used to simulate the motion of the tubes. Safeguards were implemented to reduce instabilities in FSI computations by bounding the fluid pressure and wall shear stress at the fluid/solid interface. Checks were done to ensure that the interface and stress values were well within bounds to prevent artificially limiting computed figures.

The wall thickness of the vibrating tubes is 0.4 mm, while the outer diameter is 30 mm. The very thin wall for the tubes posed relatively high computational costs for meshing the hollow cylinders and interpolating quantities between the fluid and solid domains. Consequently, simulations were performed on tubes with a solid, non–hollow configuration. For instance, the number of mesh cells for hollow tubes was 900,000. On the other hand, the solid tubes had 160,000 cells. The density of the tubes with the solid configuration was rescaled to match the mass of the hollow tubes as 743.2 kg/m^3. The modulus of elasticity for the solid-tube cases was rescaled to match the experimentally measured average natural frequency of 14.18 Hz. The moduli of elasticity of the vibrating non – hollow tubes are 70 GPa and 150 GPa for Configurations n°11and n°3, respectively.

For Configuration n°11, with two flexible cylinders and a volume fraction of 34.5%, cases 2, 4 and 6 with pitch velocities of 0.93 m/s, 1.15 m/s and 1.30 m/s, respectively. Figure 199 shows the comparison of the root mean square displacement amplitude between the experiments and the simulations. The three numerical cases are in close agreement with the experiment, with the RMS vibration amplitude increasing with the higher flow pitch velocity. The closest match is the case with the lowest flow pitch velocity. The time series of the displacement of Tubes 4 and 7 for Configuration n°11 Case 2 is shown in Figure 20. For each of the Configuration n°11 cases, the displacement and frequency responses between Tubes 4 and 7 are very similar to each other, as presented in Figure 21, 22 and 23. The vibration frequency shows two peaks: the first at 17Hz –22 Hz, which is a slight overprediction of the natural

frequency in air of 14.18 Hz from the TITAN experiments. The second peak is observed around 1.5 Hz across the three cases.

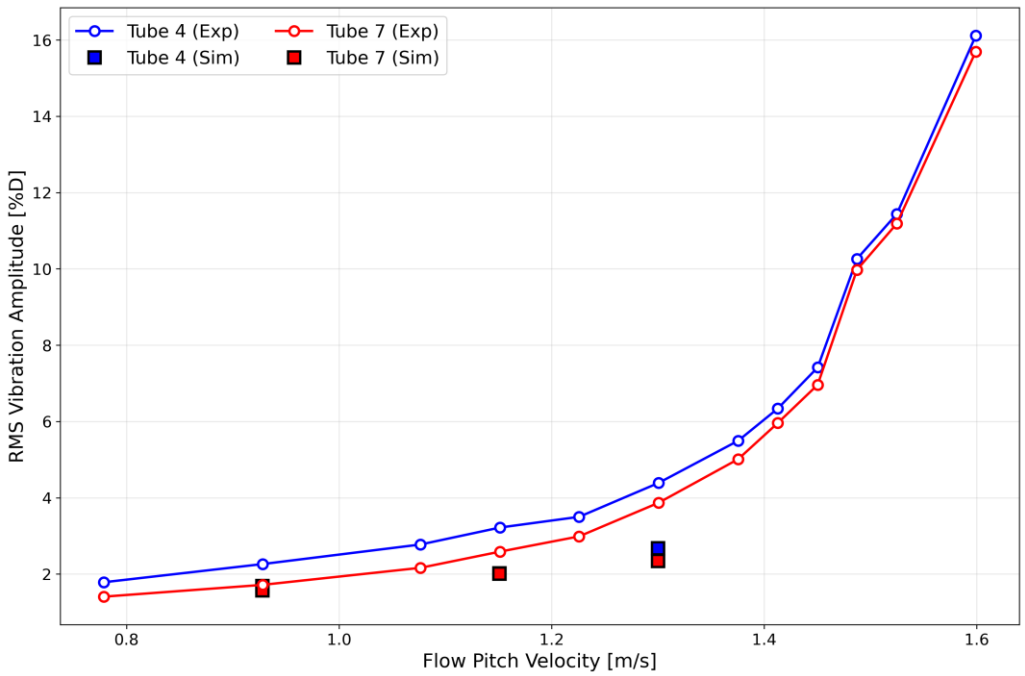

Figure 19: Configuration 11 - Comparison of the RMS amplitude of vibration versus flow pitch velocity between the simulations and the experiment data.

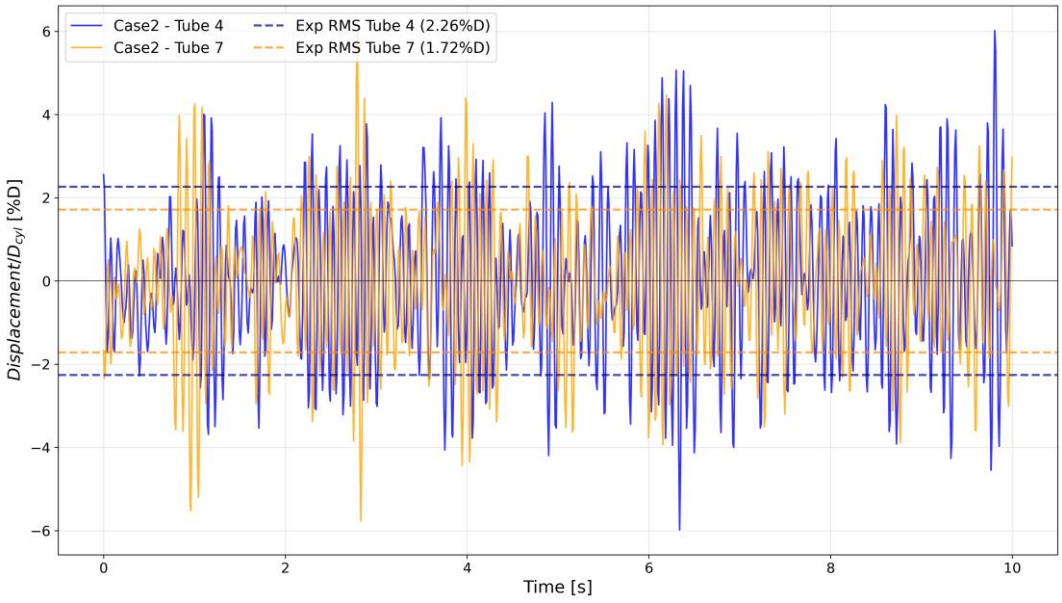

Figure 20: Configuration 11 – Case 2: Plot of the timeseries of the displacement (normalised by the diameter) of Tubes 4 and 7.

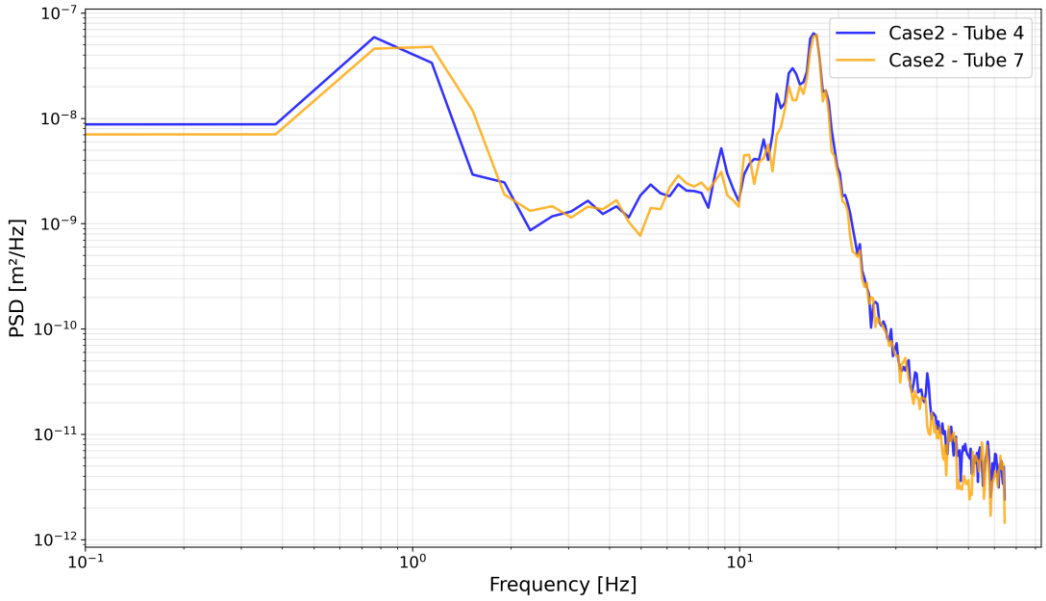

Figure 21: Configuration 11 – Case 2: PSD of the displacement of Tubes 4 and 7

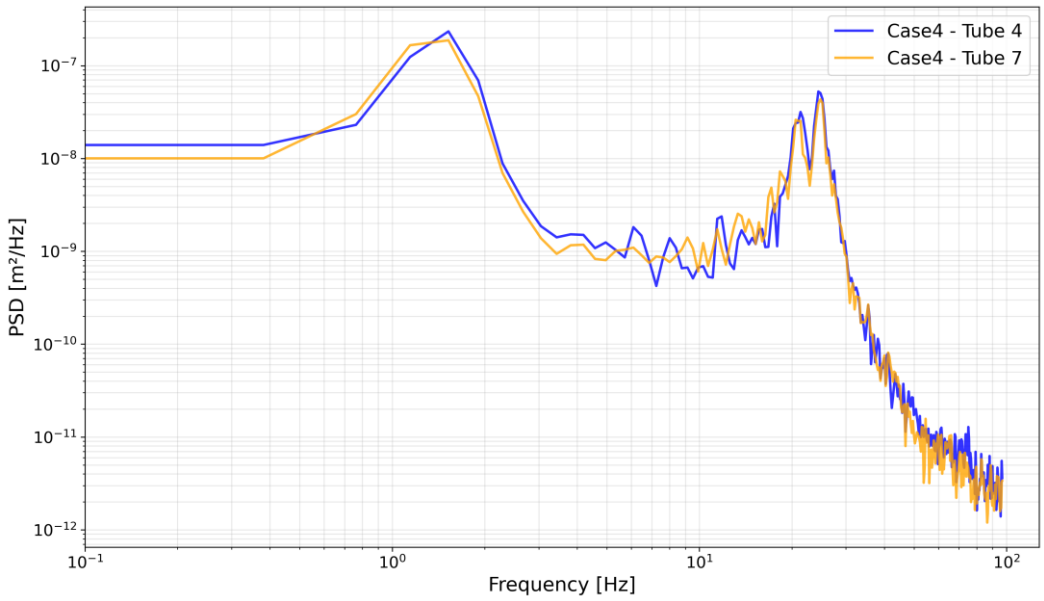

Figure 22: Configuration 11 – Case 4: PSD of the displacement of Tubes 4 and 7

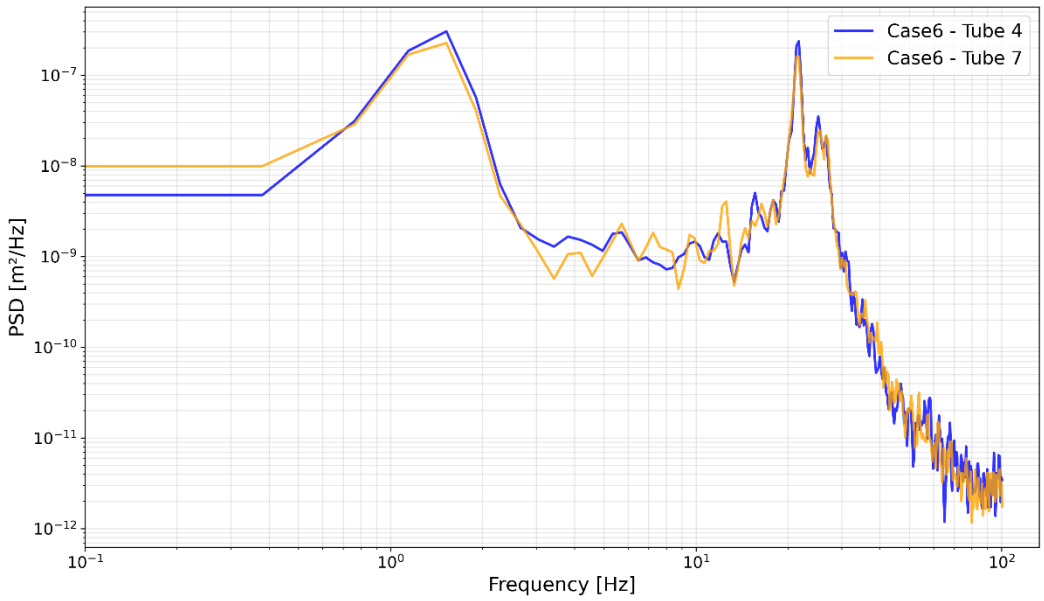

Figure 23: Configuration 11 – Case 6: PSD of the displacement of Tubes 4 and 7.

Table 4: Configuration 3 – Case 3: Comparison of RMS vibration amplitude between the experiment and the numerical simulation

	Tube 4	Tube 5	Tube 6	Tube 7	Tube 8	Tube 9	Tube 10
Exp.	1.52	1.64	1.56	1.45	1.42	1.40	1.41
Num.	1.36	1.29	1.27	1.42	1.29	1.36	1.16

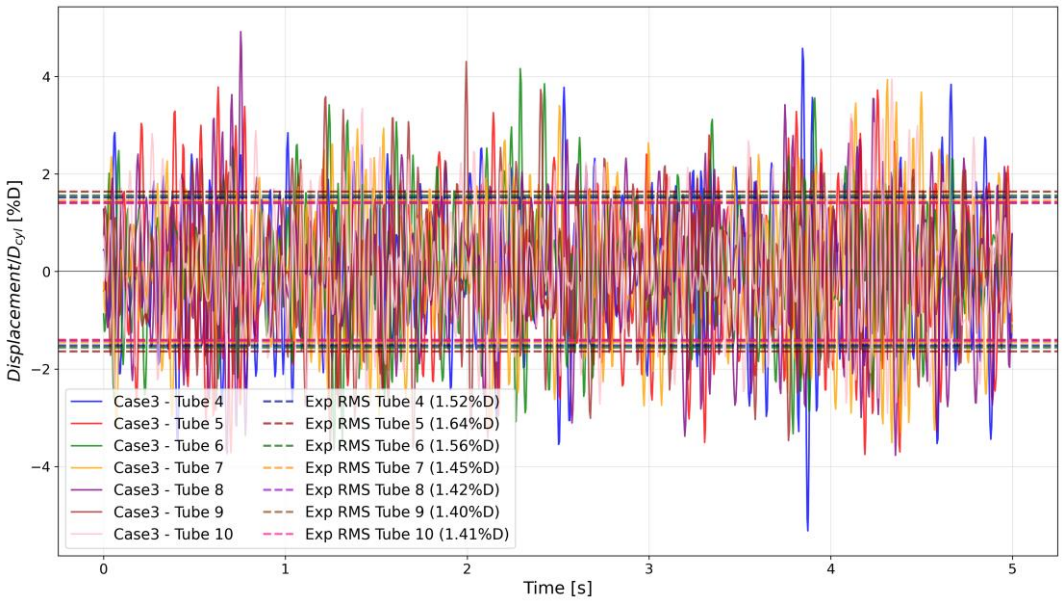

Figure 24: Configuration 3 – Case 3: Plot of the timeseries of the displacement (normalised by the diameter) of Tubes 4 to 10.

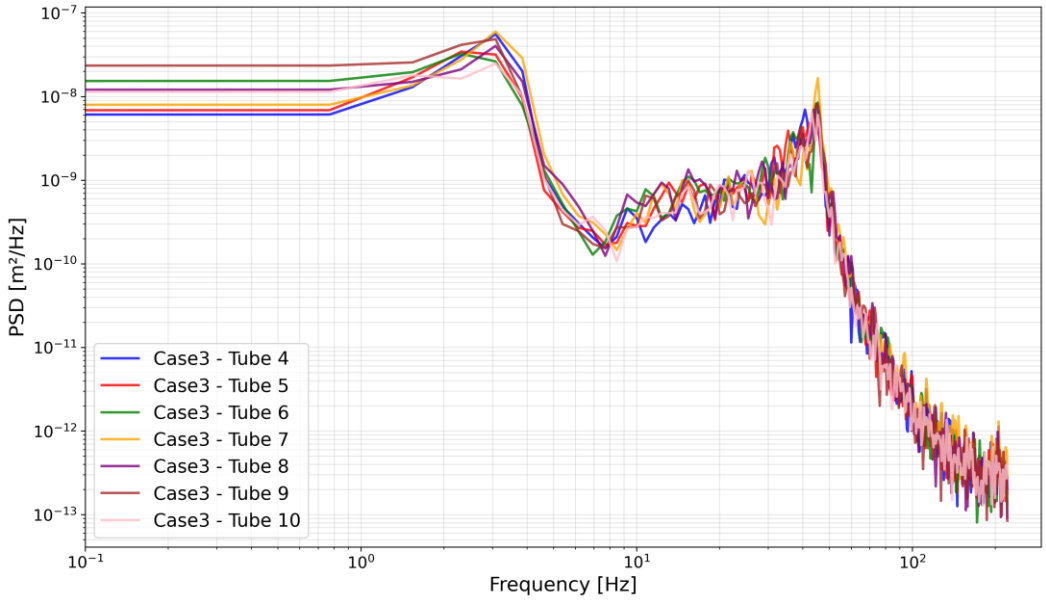

Figure 25: Configuration 3 – Case 3: PSD of the displacement of Tubes 4 to 10.

For Configuration n°3, with seven flexible cylinders and a volume fraction of 54.78%, only one simulation – Case 3 with flow pitch velocity of 1.40 m/s – was performed due to the high computational cost of modelling the fully coupled vibrations of seven tubes. The time series of displacements for Tubes 4 – 10 in Case 3 is shown in Figure 244. As previously observed, the displacement and frequency responses between the tubes are almost identical to each other, as demonstrated in Figure 255. The frequency response of the seven tubes shows two peaks: the first at 37Hz –44 Hz, which is a minor overestimation of the natural frequency in air of 31.96 Hz for Configuration n°3 from the TITAN experiments. The second peak is observed around 3.1 Hz. Table 44 shows the comparison of the RMS displacement amplitude between the experiment and numerical calculation for all seven tubes. The RMS displacement amplitude from the Case 3 simulation is in excellent agreement with the experimental result.

6. Conclusion

Considering the variety of numerical models and calculation domains, having such quantitative and qualitative similarities between simulations strengthens confidence in the numerical predictions. The triangular arrangement coupled to a slip between phases close to 1 are probably responsible of the stability of the flow and the agreement between simulation, since the flow is more restricted by the triangular arrangement geometry than in a square arrangement. Thus, having a different inlet gas size distribution than the experiment appears to be less predominant after a few rows in the tube bundle than for the square arrangement. This finding is of great interest since there is no information on the gas size distribution from the experiment at the inlet except the flow rates. Finally, the present result shows for different homogenous void fraction and mass flow rates a correct agreement from three different partner contributions with the experiment in terms of void fraction and force prediction. Further, the use of resolved approach for large gas structure appears to be the main parameter to get correct force spectra. The conclusions of the flexible configuration are in agreement and highlight that it is possible to predict two-phase flow-induced vibration in tube bundles.

Bibliography

[1] P. Piteau, X. Delaune, D. Panunzio, R. Lagrange, J. Antunes, Experimental investigation of in-flow fluidelastic instability for rotated triangular tube bundles subjected to single-phase and two-phase transverse flows, Journal of Fluids and Structures, Volume 123, 2023.

[2] D. Panunzio, R. Lagrange, P. Piteau, X. Delaune, J. Antunes, Experimental investigation of out-of-flow fluidelastic instability for rotated triangular bundles subjected to single-phase and two-phase transverse flow. Proceedings of the Flow Induced Vibration conference, Paris-Saclay, 2022.

[3] Delhaye, J., 1974. “Jump conditions and entropy sources in two-phase systems. local instant formulation”. International Journal of Multiphase Flow, Vol. 1, No. 3, pp. 395–409.

[4] Ishii, M. and Hibiki, T., 2011. Thermo-fluid dynamics of two-phase flow (Second edition). Springer New York. ISBN 9781441979841.

[5] Merigoux N., “Multiphase Eulerian-Eulerian CFD supporting the nuclear safety demonstration“. Nuclear Engineering and Design, 2022, Volume 397, , 111914.

[6] Benguigui, W., Benhamadouche, S., Beltran, F. and Hassan, M., 2024. “Experimental and numerical contributions on flow-induced vibration in steam-generator-like tube bundles: A review”. Nuclear Engineering and Design.

[7] Hirt, C. a. (1981). Volume of Fluid (VOF) Method for the Dynamics of Free Boundaries. *Journal of Computational Physics*, 201–225.

[8] Ishii, M. (1975). *Thermo-fluid Dynamic Theory of Two-phase Flow.* Eyrolles.

[9] Egorov, Y. M. (2014). Development of an effective two-equation turbulence modeling for CFD of large-scale interface in two-phase flows. *Proceedings of the 12th International Conference on Nuclear Thermal Hydraulics (NURETH-12).* Pittsburgh, PA.

[10] Brackbill, J. K. (1992). A continuum method for modeling surface tension. Journal of Computational Physics. *Journal of Computational Physics*, 335-354.

[11] H. Dolfen and J. Degroote. A synthetic bubble model as inlet for fluid-structure interaction simulations with two-phase flow. In 9 th European Congress on Computational Methods in Applied Sciences and Engineering, pages 1–13, Lisbon, Portugal, 3–7 June 2024.

[12] T. Höhne, E. Krepper, G. Montoya, D. Lucas. Experiments and numerical simulations of horizontal two-phase flow regimes. In: Proceeding of the Seventh International Conference on CFD in the Minerals and Process Industries. Melbourne, Australia, 2009.

[13] Deendarlianto et al.. Application of a new drag coefficient model at CFD-simulations on free surface flows relevant for the nuclear reactor safety analysis. Annals of Nuclear Energy, Vol. 39 70-82, 2012.

[14] T. Höhne, P. Porombka, S. Moya Saez. "Validation of AIAD sub-models for advanced numerical modelling of horizontal two-phase flows". Fluids. 5(3). 2020.

[15] Hansch, S., D. Lucas, E. Krepper, T. Hohne. CFD-simulation of boiling in a heated pipe including flow pattern transitions using the GENTOP concept. Nucl. Eng. and Des., Vol. 322, 165-176, 2017.

[16] Ansys Fluent Theory Guide, Release 2024 R1. Ansys, Inc. 2024

[17] M. Ishii, N. Zuber, Drag coefficient and relative velocity in bubbly, droplet or particulate flows, AIChE journal, 25 (1979), pp. 843-855, 10.1002/aic.690250513.

[18] A. Tomiyama, Struggle with computational bubble dynamics, Multiphase Science and Technology, 10 (1998), pp. 369-405, 10.1615/MultScienTechn.v10.i4.40

[19] S.P. Antal, R.T. Lahey Jr, J.E. Flaherty, Analysis of phase distribution in fully developed laminar bubly two-phase flow, Int. J. Multiph. Flow, 17 (5) (1991), pp. 635-652.

[20] Burns, A.D., Frank, T., Hamill, I., Shi, J.-M., et al., 2004. The Favre averaged drag model for turbulent dispersion in Eulerian multi-phase flows. In: 5th International Conference on Multiphase Flow, Vol. 4, ICMF, pp. 1–17

[21] Frederix E.M.A., Cox T.L.W., Kuerten J.G.M., Komen E.M.J. Poly-dispersed modeling of bubbly flow using the log-normal size distribution